

# Different Approaches Used for Modeling and Simulation of Polymer Electrolyte Membrane Fuel Cells: A Review

Muhammad Arif,\* Sherman C. P. Cheung, and John Andrews



Cite This: *Energy Fuels* 2020, 34, 11897–11915



Read Online

ACCESS |

Metrics & More

Article Recommendations

**ABSTRACT:** Modeling and simulation play a very crucial role in the development of the polymer electrolyte membrane (PEM) fuel cells. This review presents a detailed literature overview of the approaches used for PEM fuel cell modeling and problems related to it. The review starts with a brief overview of the hydrogen energy storage system and working of PEM fuel cells. After that, the models range from a simplified one-dimensional model to full three-dimensional models that are used to simulate the PEM fuel cells and are elaborated. The issues associated with the experimental validation of the model, especially in the concentration loss regions of the polarization curve, are also discussed. In addition to that, the physical interpretation of the ANSYS PEM fuel cell module governing equations are explained in terms of the practical processes taking place within PEM fuel cells. Finally, the gaps identified in the current knowledge of the PEM fuel cell simulation modeling are highlighted.

## 1. INTRODUCTION

To minimize CO<sub>2</sub> emissions, renewable energy sources should be used to produce electricity, to reduce the global reliance on fossil fuels for future generations.<sup>1</sup> Despite the unreliable nature of renewable energy sources, one of the major challenges that renewable energy sources are facing to replace fossils is balancing between demand and supply.<sup>2</sup> To tackle this issue, great efforts have been made, but the most promising solution among all is an electric energy storage system.<sup>3</sup> The different approaches used for storage of electrical energy are given in Figure 1.

Hydrogen is now one of the most efficient vectors of energy to store, transport, and deliver vast quantities of energy at the scales ranging from gigawatt hour to terawatt hour.<sup>4</sup> Nowadays, a hydrogen-based energy storage system (shown in Figure 2) is considered desirable as a result of its pollution-free transport, the capacity to store good energy content, and most significantly, the availability of renewable energy and water supplies.<sup>5</sup> As shown in Figure 2, the water is dissociated into oxygen and hydrogen through an electrolyzer, using the direct current (DC) electricity generated from solar energy by photovoltaic cells. Hydrogen is then compressed and supplied to the fuel cell to produce electricity.

Fuel cells are emerging as a potential key component in hydrogen-based electrical energy storage systems in the 21st century.<sup>7–9</sup> A fuel cell is an electrochemical device that generates electricity with zero carbon emission while using hydrogen as a fuel.<sup>10</sup> Fuel cells are categorized into different types depending upon the type of electrolyte used: alkaline, microfluidic, and solid oxide.<sup>11</sup>

Among these types, polymer electrolyte membrane (PEM) fuel cells are receiving increasing interest for use in environmentally friendly electrical energy storage systems.<sup>12</sup> PEM fuel cells comprise several distinguishing properties compared to other types of fuel cells, such as low operating

temperature (about 80 °C), quick start, and high current densities. Such properties make PEM fuel cells an emerging alternative of power generation in the field of automotive, power production, and electronics.<sup>13</sup>

A standard single PEM fuel cell is assembled of the following components:<sup>11</sup> (a) Bipolar plates (BPs): A single PEM fuel cell contains two bipolar plates, one on each side. They are used to collect electrons and are mostly made of SS-316 material. Graphite is also one of the best options for excellent performance, but the machining process required for the grooving of the gas flow channels is quite expensive.<sup>14</sup> Aluminum is also considered as an ideal material for the manufacturing of the bipolar plates of the cell as a result of its less weight and high mechanical strength.<sup>15</sup> (b) Gas flow channels (GFCs): These are grooved in the bipolar plates for the reactant and oxidant supply to the electrodes and extraction of water out of electrodes. (c) Gas diffusion layers (GDLs): These are the porous medium used to distribute the species gases uniformly over the surface of catalyst layers. Carbon-based GDLs are widely used because of their properties, such as high stability in an acidic environment, high electrical conductivity, and higher gas permeability. There are some metal-based GDLs, such as metal mesh, metal foam, and micromachined metal substrate, used in the PEM fuel cells as a result of good mechanical strength and high stability over a wide potential range.<sup>16</sup> (d) Catalyst layers (CLs): These are thin surface layers used to provide the sites for electrochemical

Received: July 19, 2020

Revised: September 10, 2020

Published: September 15, 2020



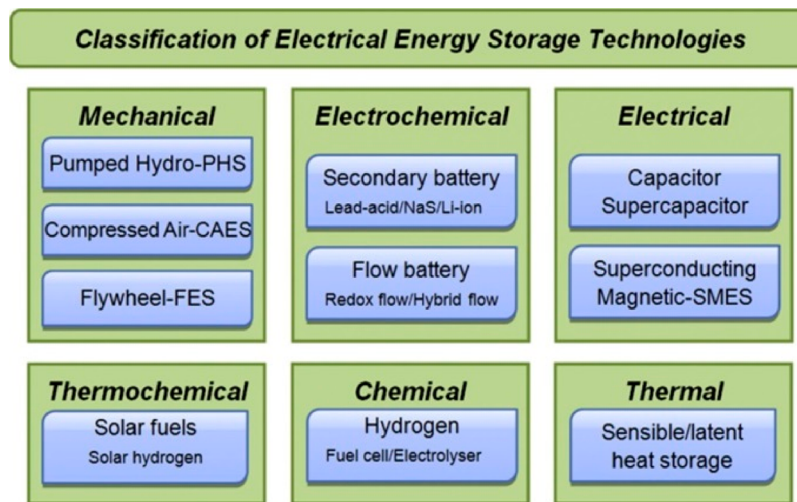


Figure 1. Classification of different electrical energy storage system technologies.<sup>2</sup>

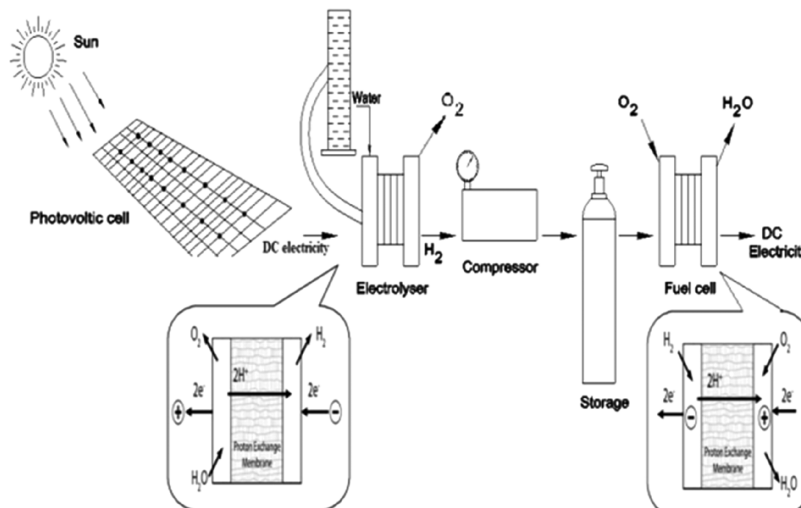


Figure 2. Schematic of a conventional hydrogen system.<sup>6</sup>

reactions in fuel cell and electrolyzer modes. Platinum and platinum alloys are widely used as a catalyst for the electrochemical reactions taking place in the PEM fuel cells. (e) Membrane: A single polymer electrolyte membrane is impermeable for species gases and electronic insulators, allowing for the passage of protons only. Generally, an ionomer membrane based on perfluorosulfonic acid (PFSA), such as Nafion, is one of most widely used membranes in fuel cells.<sup>17</sup>

The main components of a PEM fuel cell are depicted in Figure 3.

As presented in Figure 4, hydrogen-rich fuel is supplied through hydrogen electrode (anode side) channels, where it diffuses through GDLs and reaches the catalyst layer at the hydrogen side (anode side), where the hydrogen oxidation reaction takes place. The hydrogen molecule breaks into hydrogen protons and electrons.

The chemical reaction undergoing on the hydrogen side (anode) is

hydrogen oxidation reaction

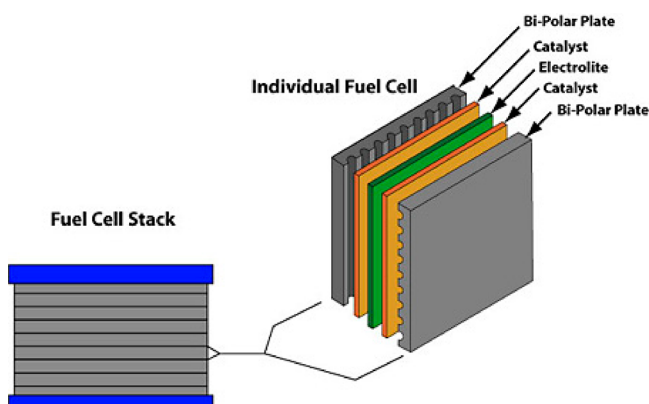
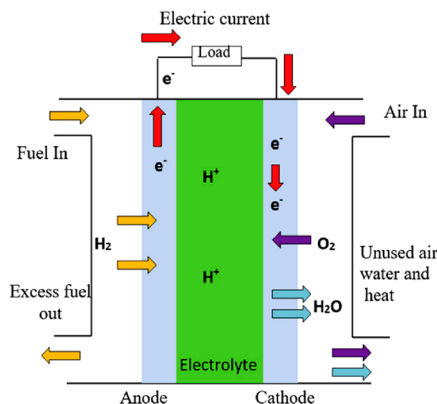


Figure 3. Schematic presentation of the main components of a PEM fuel cell.<sup>18</sup>

Protons (H<sup>+</sup>) move to the oxygen side (cathode) through the membrane, while the electron reaches there through an external circuit. Similarly, oxygen supplied through cathode channels diffuses through GDLs toward the oxygen side (cathode), where it combines with the hydrogen proton and



**Figure 4.** Schematic diagram of the working of a PEM fuel cell.<sup>19</sup> The different color codes used are to differentiate between different cell components, such as catalyst layers, GDLs, and membrane. The arrows with different colors represent the flow of hydrogen, oxygen, water, and electrons.

electron; hence, the oxygen reduction reaction takes place, and water is formed.<sup>20</sup> The electrons transferred through an external circuit are the current generated.

The chemical reaction undergoing on the oxygen side (cathode) is

oxygen reduction reaction



The overall PEM fuel cell reaction is

net reaction



The purpose of this review is to briefly survey the different approaches used for the modeling of PEM fuel cells and identify the gaps in the current knowledge and their application. The review is organized as follows: First, the different models ranging from one-dimensional (1D) to three-dimensional (3D) models that are applied to the simulation of PEM fuel cells and stacks are illustrated in detail. The different approaches and difficulties in validating the models experimentally are also elaborated. After that, various commercial codes applied for the simulation and modeling of the PEM fuel cells are discussed briefly, while the ANSYS PEM fuel cell module is explained in more detail. In the end, the limitations and gaps in the area of the simulation and modeling of the PEM fuel cells are summarized.

## 2. NUMERICAL MODELING OF PEM FUEL CELLS

### 2.1. Significance of Numerical Modeling of PEM Fuel Cells.

Fabrication and testing of PEM fuel cell prototypes are expensive processes in terms of time and cost.<sup>21</sup> The performance of PEM fuel cells has been increasingly assessed through computational fluid dynamics (CFD) modeling and simulation techniques instead of time-consuming and expensive experiments.<sup>22</sup> To analyze the PEM fuel cell performance, the understanding of the local processes taking place within the cells is very important.<sup>23</sup> As a result of the reactions that are taking place throughout the cell and compact and closed shape of the fuel cell, it is impossible to study the processes, such as water management and thermal manage-

ment, through *in situ* experiments. Modeling and simulation are one of the best approaches to study these processes.<sup>24</sup> The challenges to researchers in studying these phenomena by experiments motivated them for the development of numerical models of PEM fuel cells.

**2.2. One-Dimensional Model.** The PEM fuel cell modeling was initially started with a 1D model, and it was then expanded to two-dimensional (2D) and 3D. Springer et al.<sup>25</sup> were the first to develop a steady-state 1D isothermal model using a Nafion 117 membrane as an electrolyte, which predicted the net-water-per-proton-flux ratio under normal conditions. This model demonstrated that the use of a thinner membrane would help in overcoming the issue of overall cell resistance. The predictions made by this model were validated experimentally at different operating conditions. The model presented in this paper was unable to estimate the humidification requirements of the inlet flow gases at the cathode. Moreover, this model could not evaluate the influence of surplus liquid water on the PEM fuel cell performance, which may boost the conductivity of the membrane or may cause resistance to the transport of species gases.

Bernardi and Verbrugge<sup>26</sup> also developed a 1D model (Figure 5) for solid polymer electrolyte fuel cells to determine

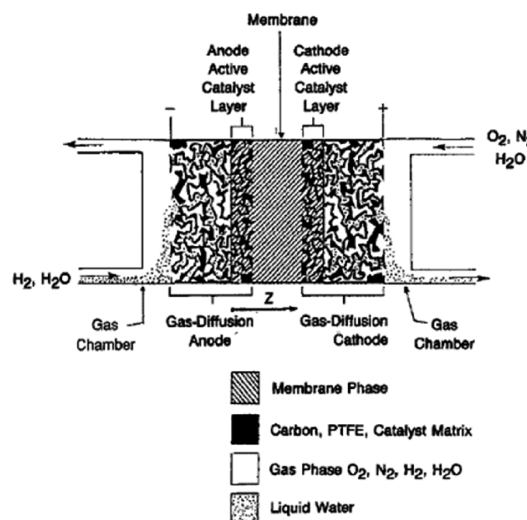


**Figure 5.** Schematic illustration of the 1D PEM fuel cell model.<sup>26</sup> This figure was reused with permission from ref 26. Copyright 1992 The Electrochemical Society.

the cell performance affecting factors and to study the mechanism of species gas transport. The study results showed that the volume fraction of the cathode electrode available for the transport of the gas should be increased to maximize the limiting current densities. This model also predicted that dehydration of the membrane could limit the PEM fuel cell performance. Predictions of this model were validated experimentally by tuning the values of the exchange current density to match the simulation results with experimental data.

Pasaogullari and Wang<sup>27</sup> developed a 1D model to analyze the effects of the wettability of GDLs, liquid water, and catalyst flooding on the PEM fuel cell performance. The study results predicted higher liquid saturation values at the catalyst layer interface for hydrophilic GDLs (contact angle,  $\theta_c$ , of  $<90^\circ$ ) than the hydrophobic GDLs (contact angle,  $\theta_c$ , of  $>90^\circ$ ).

Rahman et al.<sup>28</sup> developed a 1D non-isothermal model to predict the resistance to dry oxygen and limiting current.

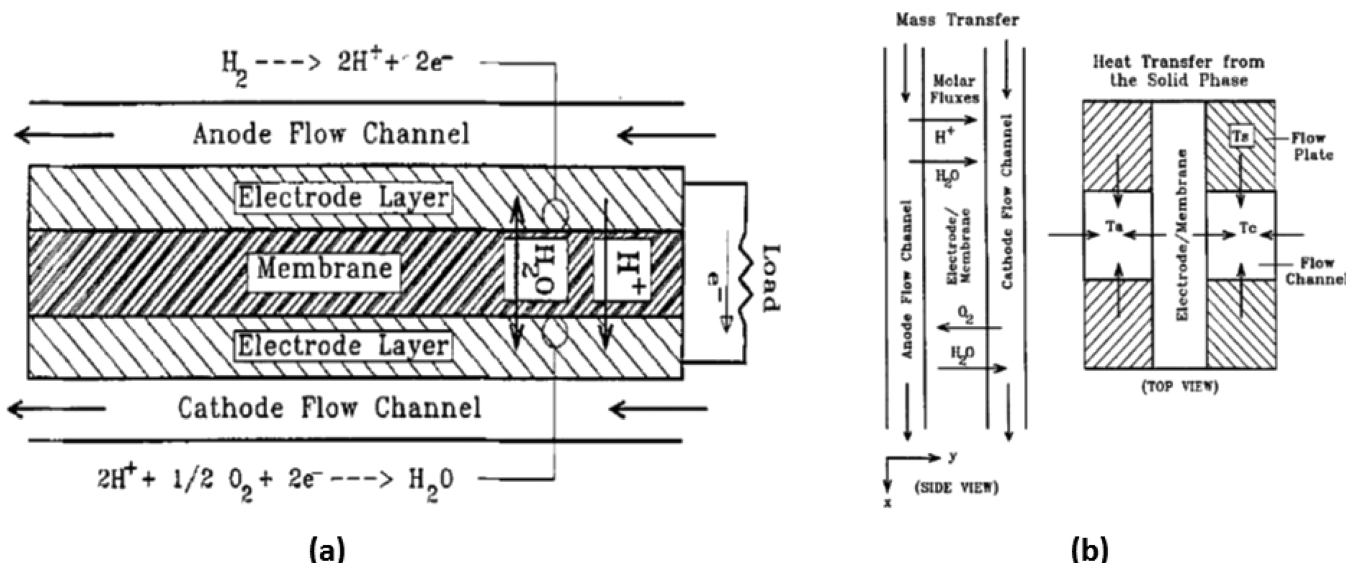


**Figure 6.** Schematic illustration of the 2D PEM fuel cell model: (a) front view and (b) side and top views.<sup>30</sup> This figure was reused with permission from ref 30. Copyright 1993 The Electrochemical Society.

Ionescu<sup>29</sup> developed a 1D model to study the net water flux and hydrogen crossover across the Nafion membrane in the PEM fuel cell. The study results showed that the cell performance improves as the cell pressure and temperature increase. The polarization curve plotted from model data was matched with the experimental data, and both results were in good agreement.

The 1D models give the most simplistic representation of the PEM fuel cell by considering the transport mechanism across the cell only. The accuracy of the model is reduced as a result of some assumptions made to simplify the model. Despite having certain limitations, 1D models are still considered as a foundation stone of the modeling of PEM fuel cells.

**2.3. Two-Dimensional Model.** The computational modeling of the fuel cells was extended to a 2D model by Fuller and Newman,<sup>76</sup> developing the 2D membrane electrode assembly for the analysis of the water and thermal management and hydrogen consumption. This model related the hydration of the membrane to the heat removal rate. Lower heat removal rates will dehydrate the membrane, which will cause a decrease in the PEM fuel cell performance. A steady-state 2D model was developed by Nguyen and White<sup>30</sup> (Figure 6) to study the thermal and water management by evaluating the effects of humidification. The results obtained from the model indicated that the ohmic polarization as a result of the membrane largely contributes to the polarization losses, at high current densities.

A 2D (along the channel) model was developed by Yi and Nguyen<sup>31</sup> to analyze the PEM fuel cell performance under different channel flow fields and operating conditions. The study results showed that increasing anode humidification and back diffusion of water through the membrane can boost the PEM fuel cell performance. The back diffusion of water through the membrane can be increased by applying a higher cathode pressure. The model also suggested the use of a counterflow heat exchanger for effective heat removal. This model assumed that liquid water exists only on the surface of the channels only with a negligible volume, while more water is generated than the water removed, which will cause condensation and flooding of the cathode, at higher current

densities. Therefore, this study could not predict the drop in cell performance as a result of the cathode electrode flooding.

Chu et al.<sup>32</sup> modeling study results show that a cell with higher GDL porosities performs better because high GDL porosities allow for more species gases to transport to the catalyst for electrochemical reaction; thus, more current is generated. However, this study was limited to the influence of porosity on the transport of species gases only, leaving the effects of the porosity on the liquid water removal, while the porosity of GDL affects mass transport losses in two ways. The diffusivity of species gases from GDL to the catalyst layer increases with increasing the porosity, as a result of which more reactants and oxidants reach the catalyst layer and, hence, more current is generated. Second, by increasing GDL porosity, the removal of liquid water also increases, thus reducing the chances of GDL pore blockage and covering of active sites of the catalyst layer. This study included the effects of porosity on the transport of the species gases only and leaving the influence of the porosity on liquid removal, which also affects the performance of the cell. A similar study was conducted by Abdollahzadeh et al.,<sup>33</sup> in which it was found that higher GDL hydrophobicity and porosity results in better cell performance.

Marr and Li<sup>34</sup> investigated the performance optimization and composition of the cathode catalyst layer structure and catalyst platinum by including both mass transport process electrochemical reaction in the PEM fuel cell. The investigation indicated that the effective utilization of the catalyst decreases at high current densities; thus, the performance of the cell will not be adversely affected if lower platinum loadings are used at high current densities.

Siegel et al.<sup>35</sup> built a 2D steady state model for analyzing the influence of inlet gas velocities and the membrane conductivity on the PEM fuel cell performance. This model included equations for the transport of reactants, liquid water transport through porous electrodes, hydrogen ions, and dissolved water through the membrane. The model estimated the values for the inlet velocities of reactant gases and proton conductivity that gave the best match with experimental data.

Weber et al.<sup>36</sup> developed a model to study the influence of the flooding on the PEM fuel cell performance. The model results indicated that hydrophobic GDL reduces the chances of the GDL flooding, hence enhancing the PEM fuel cell performance at higher current densities. In this study, the effects of the covering of active sites by liquid water on the performance of the fuel cell were ignored.

Pasaogullari et al.<sup>37</sup> used a multiphase mixture approach to develop a two-phase model to study the transport of two phases within the microporous layer (MPL). The influence of MPL properties, e.g., median pore size, porosity, thickness, and wettability, on the transport of liquid water was studied using this model. The study results showed that, by adding MPL, the water back diffusion to the anode is increased as a result of an increase in the hydraulic pressure difference across the membrane. It was also indicated that an increase in hydrophobicity and thickness of MPL could increase back diffusion of water, while decreasing the pore size and porosity of MPL will also enhance the liquid water back diffusion.

Fontana et al.<sup>38</sup> employed a 2D isothermal model to study the transport of the liquid water in the tapered gas flow channels. The study results show that the velocity of air influences the transport and liquid water distribution inside the channels.

Two-dimensional models give more detailed illustration of the PEM fuel cell and consider the transportation mechanism either across the channels or along the channels at a time. The results obtained from 2D models are considered more accurate compared to the 1D models, but the computational time and cost increased in comparison to the 1D models.

**2.4. Three-Dimensional Model.** With time, the modeling of the PEM fuel cells was further extended to more detailed models, i.e., 3D models. Dutta and Shimpalee<sup>39</sup> predicted the behavior of the temperature inside the PEM fuel cell channels and studied the influence of heat evolved during the chemical reaction on the PEM fuel cell performance using a 3D mathematical model with energy equations for the first time. A control volume method with heat production source terms, transport equations, and phase changes were used in the model. The model results show that the rise in the cell temperature as a result of electrochemical reactions influence the performance of the cell.

A 3D model was developed by Mazumder and Cole<sup>40</sup> with equations governing the liquid water transport and formation inside the PEM fuel cells. The performance predicted by the model could be overpredicted if the liquid water formation is excluded. Hence, the inclusion of the transport of liquid water and formation equations in the model is critical to predict the PEM fuel cell performance accurately and to match the numerical model polarization curve with an experimental curve.

A 3D single-phase model was developed by Berning and Djilali<sup>20</sup> to investigate the transport processes in the gas flow channels and GDLs of both electrodes. The model did not include the water phase change process. However, the model was capable of analyzing the water transport and mass transport losses in detail. The modeling results and experimental data were compared, and good agreement was obtained.

A two-phase transport model in 3D was constructed by Ye and Nguyen<sup>41</sup> (Figure 7) for the prediction of the liquid saturation in the catalyst layers and GDLs of the PEM fuel cell. The modeling results indicated that the capillary pressure has a

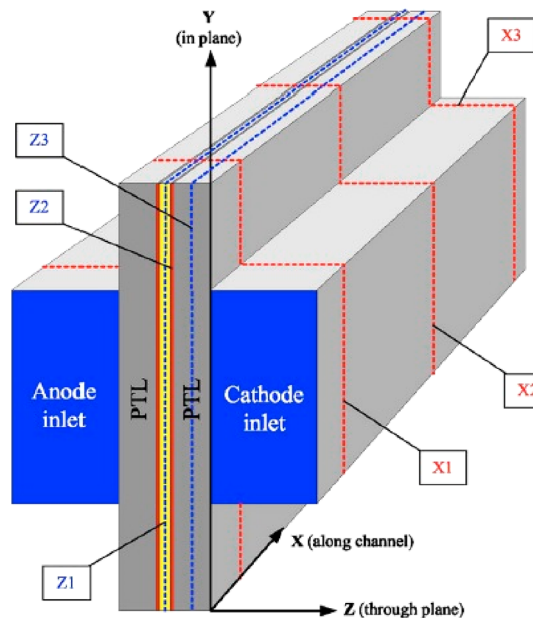


**Figure 7.** Schematic illustration of the 3D PEM fuel cell model.<sup>41</sup> This figure was reused with permission from ref 41. Copyright 2007 The Electrochemical Society.

vital role in the transport and distribution of the liquid water inside PEM fuel cell. The influence of the liquid water on the oxygen transport predicted by the single-phase model was compared to the same effects predicted by the two-phase model. In the single-phase model, the effects of liquid saturation “s” on the effective diffusivity of the species gases in the GDLs and catalyst layers were neglected, while in the two-phase model, these effects were included. This study also concluded that the effects of the liquid water are not properly predicted by the single-phase model and, hence, overestimates the PEM fuel cell performance.

Meng<sup>42</sup> formulated a two-phase mixed domain non-isothermal model to analyze the issues associated with the thermal and water management by involving the process of evaporation and condensation. The model was able to determine the suitable values for the coefficients of condensation and evaporation rate. The results of numerical simulation of this model indicated that liquid water is largely generated in the two regions of GDL: one near the end plates and another inside GDL but not close to the catalyst.

Berning<sup>43</sup> used a 3D multi-fluid model to analyze the multiphase flow through the porous cathodic electrode of the PEM fuel cell. The model explained the transport and liquid water saturation level inside the cathode electrode. The primary goal of this analysis was to highlight the microporous layer effects on water management inside the PEM fuel cell. The study predicted that including the microporous layer in the simulation may form a thin liquid water film at the interface of GDL/MPL.

Harvey et al.<sup>44</sup> used a 3D CFD model to compare various approaches that are applied for the modeling of catalyst layers in the PEM fuel cell: a thin film model, a discrete catalyst model, and an agglomerate model. It was found that the thin-film model overpredicts the PEM fuel cell performance compared to the other two catalyst approaches. The results of this study showed that the discrete model does not consider the dissolution of oxygen in the electrolyte phase. According to

this study, the agglomerate catalyst model has the capability of considering all of the polarization regions, including the sharp drop in the voltages as a result of concentration losses at higher currents.

Berning et al.<sup>45</sup> applied a multi-fluid approach to develop a model that explains the liquid water flow from GDLs to the gas flow channels in the PEM fuel cell. The model was used to study the influence of contact angles, porosity, and permeability on the liquid saturation in the GDL, catalyst layer and microporous layer. It was found that hydrophobicity has a minimal influence on the saturation level of liquid water.

A single-phase 3D model was used by Dawes et al.<sup>46</sup> to examine the water flooding effects on the performance of the PEM fuel cell. This model was an improved version of the previous single-phase models because it was capable of predicting the drop in performance as a result of liquid water. It was assumed that the species gases in the porous media are transported through diffusion, and therefore, effective diffusivity model was applied in the porous media. This study concluded that GDL permeability has negligibly influenced the PEM fuel cell performance because the flow of gases is highly dependent upon the diffusion.

Yuan et al.<sup>47</sup> developed a 3D multiphase model for the prediction of the effects of the operating conditions, such as the pressure, temperature of a cell, air stoichiometric ratio, and relative humidity of reactants, on the PEM fuel cell performance. The study results indicated that the PEM fuel cell performance could be boosted by raising the operating pressure and temperature. An increase in the cell temperature will evaporate the liquid water, which will decrease the flooding chances of the cathode. The increase in the performance as a result of an increase in the temperature can only be achieved if the inlet gases are adequately humidified; otherwise, the rise in the cell temperature will dehydrate the membrane and result in a performance drop. Moreover, the results of the study showed that the humidification of the anode is more critical than humidification of the cathode because electro-osmotic drag can dry out the membrane more quickly on the anode side.

Golpaygan et al.<sup>48</sup> developed a 3D multiphase model to examine the flow dynamics of water droplets in a single channel. It was found that the presence of the liquid water in the gas flow channels can cause the flow of reactants, as a result of which the pressure drop will be increased. The rise in the pressure drop will reduce the cell performance because the airflow to the catalyst active sites will be affected.

Inamuddin et al.<sup>49</sup> used a 3D single-phase model to examine the influence of the thickness and porosity of GDL on the performance of the fuel cell. The study results showed that the cell performance becomes improved with increasing the GDL porosity as a result of the increase in the species concentration at reaction sites. Similarly, by increasing the GDL thickness, the catalyst will obtain more reactants as a result of the rise in the concentration gradient.

Ferreira et al.<sup>50</sup> constructed a hybrid 1D + 3D model and applied the volume of fluid (VOF) method for simulating two-phase flow of air and water in the cathode gas flow channels. The model was validated experimentally, and both results were in good agreement. Ashrafi and Shams<sup>51</sup> employed a 3D model using the VOF method to assess the influence of the orientation of the flow channel configuration on the water management in the PEM fuel cell.

Zhang and Jiao<sup>52</sup> developed a 3D multiphase model by coupling the Eulerian–Eulerian model and two-phase model.

The two-fluid model was applied to porous electrodes, while gas and two-phase liquid flows in the channels were solved using the Eulerian–Eulerian model. The model included the evaporation and condensation of liquid water in gas flow channels and the effects of the gravitational forces.

Li and Sundén<sup>53</sup> applied a 3D two-phase flow model to study the effects of deformation of GDL on the transport process and the performance of the fuel cell. The study illustrated that the performance of the cell improves with increasing assembly pressure but also increases the pressure drop in the flow channels. Hence, it is recommended to reduce the assembly pressure to reduce parasitic losses.

Havaej et al.<sup>54</sup> applied a 3D two-phase flow model to examine the influence of the non-uniform distribution of catalyst loadings on cathode half-cell performance. The study findings illustrated that the influence of the catalyst distribution was higher at higher current densities and less at lower current densities.

Li et al.<sup>55</sup> built a 3D non-isothermal two-phase flow model to examine the PEM fuel cell performance with a thin membrane electrode assembly operating under lower humidity conditions. This study also explained the influence of oxygen transport resistance and reduction of the catalyst on the automotive PEM fuel cell performance at high current densities. This modeling study predicted that a thin electrolyte membrane has lower ohmic resistance and can be easily hydrated under low humidity conditions compared to the thicker membrane.

Thosar et al.<sup>56</sup> derived an analytical model for the PEM polarization curve considering a low humid PEM fuel cell. This analytical model also explained a technique to find the *in situ* oxygen diffusion coefficients at different conditions. The parameters estimated by this model was matched with experimental data, and both results were in good agreement.

Wilberforce et al.<sup>57</sup> investigated the design of the existing geometry of the bipolar plate with reference to the maximum PEM fuel cell performance. This study also explained some of the key design parameters of bipolar plate geometry, such as channel length, flow direction, and use of baffles, that can increase the PEM fuel cell performance. The results were beneficial for selecting the best bipolar plate geometry.

Atyabi et al.<sup>58</sup> developed a multiphase model 3D to analyze the cell assembly pressure effects on the contact resistance between bipolar plates and GDL. These results showed that the contact resistance between bipolar plates and GDL declines as the assembly pressure increases, which results in better cell performance. This study also revealed that, with an increase in the cell assembly pressure, the temperature of the cell also rises; as a result of electrochemical reaction heat source, the rise in the cell temperature was higher on the cathode side.

Carcadea et al.<sup>59</sup> studied the effects of the composition and properties of the catalyst layer, such as platinum loadings, particle radius ionomer, volume fraction, electrochemical active surface, and mass transport resistance from liquid water and ionomer covering particles of the catalyst, on the PEM fuel cell performance. This study concluded that higher cell performance can be obtained with a smaller particle size and higher platinum loadings. The optimum range predicted by the model for the volume fraction of ionomer was from 45 to 55% that leads to a 39% gain in the overall fuel cell performance. The simulation results were a good match with experimental data.

Han and Chen<sup>60</sup> studied the effects of the air velocity and wettability by simulating a generalized 2D model with the VOF method. The results obtained from the numerical simulation indicated that the wettability of the GDL material is more effective than the mass flow rate of liquid water to penetrate into the GDL. The model results also showed that adequate hydrophobicity and high air velocity in gas flow channels can assist the liquid water droplet removal from the GDL surface.

Havaej<sup>61</sup> applied a 3D two-phase flow model to study the effects of the configuration of the converging–diverging channel on the PEM fuel cell performance. It was depicted that converging–diverging channels were more effective at higher current densities and boosted the performance by 10% compared to straight channels.

Li et al.<sup>62</sup> used a 3D model to study the PEM fuel cell performance with a thin membrane operating under low humidity. The study results showed that the thin membrane has low ohmic losses and can be easily hydrated, even at lower humidity, but on the other side, the chance of hydrogen crossover is higher.

Xie et al.<sup>63</sup> developed a combined “1D + 3D” model, in which the 1D domain was applied to catalyst layers, membrane, and GDL on the anode side, while the 3D domain incorporated flow channels and cathode side GDL. It was found that using the “1D + 3D” model reduces the computational cost and time compared to full 3D modeling.

Zhang et al.<sup>64</sup> applied the 3D multiphase model to study the spatial distribution of the current density at different temperatures, voltages, relative humidity (RH), and current density. The model was validated by comparing the simulated polarization curve and current density distribution to experimental polarization curve and current density distribution data, respectively. It was found that, under 50% RH conditions, current density values are higher at the cathode inlet, while for 25% RH, the higher values shifted to the middle of the cell.

Generally, in the fuel cell modeling, details such as current density contours, temperature contours, and species velocity profiles cannot be obtained by simplistic 1D and 2D simulations. Three-dimensional models give the most realistic representation of the fuel cell by taking into account the transport mechanisms across all of the planes. The results obtained from the 3D models are more realistic compared to the results obtained from 1D and 2D models. The computational time and cost required for the 3D modeling are high, which is considered as its downside compared to 1D and 2D models (Tables 1–3).

**2.5. Modeling of Stacks.** CFD-based modeling was further widened to the performance assessment of multi-cell stacks. Shan<sup>65</sup> developed a layer-based 1D for a 10 cell stack, in which the components of the cell, such as gas flow channels, GDLs, catalyst layers, and membrane, were considered as layers. Similarly, Gao et al.<sup>66</sup> also developed a 1D multiphysics dynamic model for the simulation of the PEM fuel cell stack using VHDL-AMS modeling language. In this model, each cell is divided into layers called “elementary layers” based on their positions, functions, and geometry.

Wöhr et al.<sup>67</sup> developed a 2D transport model for thermal and water management in a single cell and PEM stack made up of four single cells. The study results indicated that increasing porosity and decreasing thickness of GDL could help the water to diffuse toward the anode side of the membrane to hinder the dehydration of the membrane. This study also suggested

conservation equation	two-dimensional model <sup>b</sup>	three-dimensional model <sup>c</sup>	three-dimensional multiphase model <sup>d</sup>
mass	$\nabla(\rho\vec{u}) = S_m$	$\nabla(\rho\vec{u}) = S_m$	$\nabla(1-s)(\rho_g\vec{u}) = S_m;$ (gas)
momentum	$\nabla(\rho\vec{u}_i) = \nabla(\mu\nabla u_i) - \frac{\partial P}{\partial i} + S_i;$ $i = x, y, z/y, z$	$\nabla(\rho\vec{u}_i) = \nabla(\mu\nabla u_i) - \frac{\partial P}{\partial i} + S_i;$ $i = x, y, z$	$\nabla(1-s)(\rho_g\vec{u}_i) = \nabla(\mu\nabla u_i) - \frac{\partial g}{\partial i} + S_i;$ $i = x, y, z$ (gas)
hydrogen	$\nabla(\rho\vec{u}Y_{H_2}) = \nabla(\rho D_{H_2}^{\text{eff}}\nabla Y_{H_2}) + S_{H_2}$	$\nabla(\rho\vec{u}Y_{H_2}) = \nabla(\rho D_{H_2}^{\text{eff}}\nabla Y_{H_2}) + S_{H_2}$	$\nabla(\rho\vec{u}Y_{H_2}) = \nabla(\rho D_{H_2}^{\text{eff}}\nabla Y_{H_2}) + S_{H_2}$
oxygen	$\nabla(\rho\vec{u}Y_{O_2}) = \nabla(\rho D_{O_2}^{\text{eff}}\nabla Y_{O_2}) + S_{O_2}$	$\nabla(\rho\vec{u}Y_{O_2}) = \nabla(\rho D_{O_2}^{\text{eff}}\nabla Y_{O_2}) + S_{O_2}$	$\nabla(1-s)(\rho\vec{u}Y_{O_2}) = \nabla(\rho D_{O_2}^{\text{eff}}\nabla Y_{O_2}) + S_{O_2}$
water vapor	$\nabla(\rho\vec{u}Y_{wv}) = \nabla(\rho D_{wv}^{\text{eff}}\nabla Y_{wv}) + S_{wv} + S_{WPYLV} - S_{WDYWD}$	$\nabla(\rho\vec{u}Y_{wv}) = \nabla(\rho D_{wv}^{\text{eff}}\nabla Y_{wv}) + S_{wv}$	$\nabla(1-s)(\rho\vec{u}Y_{H_2O}) = \nabla(\rho D_{H_2O}^{\text{eff}}\nabla Y_{H_2O}) + S_{H_2O}$
electric charge	$\nabla(\sigma_{\text{slid}}\nabla\phi_{\text{slid}}) + S_{\phi_{\text{slid}}} = 0$	$\nabla(\sigma_{\text{slid}}\nabla\phi_{\text{slid}}) + S_{\phi_{\text{slid}}} = 0$	$\nabla(\sigma_{\text{add}}\nabla\phi_{\text{add}}) + S_{\phi_{\text{add}}} = 0$
ionic charge	$\nabla(\sigma_i\nabla\phi_i) + S_{\phi_i} = 0$	$\nabla(\sigma_i\nabla\phi_i) + S_{\phi_i} = 0$	$\nabla(\sigma_i\nabla\phi_i) + S_{\phi_i} = 0$
energy	$\nabla(\rho c_i\vec{u}T) = \nabla(k_i^{\text{eff}}\nabla T) + S_T$	$\nabla(\rho c_i\vec{u}T) = \nabla(k_i^{\text{eff}}\nabla T) + S_T$	$\nabla(\rho c_i\vec{u}T) = \nabla(k_i^{\text{eff}}\nabla T) + S_T$

<sup>a</sup>Symbols are defined at the end of the review in the Nomenclature section. <sup>b</sup>From ref 41. <sup>c</sup>From ref 35. <sup>d</sup>From ref 41. From ref 61.

**Table 1. Governing Equations Used for PEM Fuel Cell Modeling<sup>a</sup>**

Table 2. Source Terms

source term	two-dimensional model <sup>a</sup>	three-dimensional model <sup>b</sup>	three-dimensional multiphase model <sup>c</sup>	units
mass	$S_m = S_{H_2} + S_{O_2} + S_{LV} + S_{WP/LV} - S_{WD/WD}$	$S_m = S_{H_2} + S_{O_2} + S_{ww}$	$S_m = S_{O_2} + S_{H_2O}$	$\text{kg m}^{-3} \text{s}^{-1}$
momentum	$S_i = -\frac{\mu}{K_i^g} u_i$	$S_i = -\frac{\mu}{K_i^g} u_i$	$S_i = -(1-s) \frac{\mu_g}{K_i^g} u_i$	$\text{kg m}^{-2} \text{s}^{-2}$
hydrogen	$S_{H_2} = -\frac{j}{2F} M_{H_2}$	$S_{H_2} = -\frac{j}{2F} M_{H_2}$	$S_{H_2} = -\frac{j}{2F} M_{H_2}$	$\text{kg m}^{-3} \text{s}^{-1}$
oxygen	$S_{O_2} = -\frac{j}{4F} M_{O_2}$	$S_{O_2} = -\frac{j}{4F} M_{O_2}$	$S_{O_2} = -\frac{j}{4F} M_{O_2}$	$\text{kg m}^{-3} \text{s}^{-1}$
water production	$S_{WP} = -\frac{j}{2F} M_W$	$S_{WP} = -\frac{j}{2F} M_{H_2O}$	$S_{H_2O} = \frac{j}{2F} M_{H_2O} + \frac{\beta j}{2F} M_{H_2O} - S_{g-l} - M_{H_2O} S_{v-d}$	$\text{kg m}^{-3} \text{s}^{-1}$
electric charge	$S_{\phi_{\text{ild}}} = \begin{cases} -j & (\text{CL}_{\text{anode}}) \\ +j & (\text{CL}_{\text{cathode}}) \end{cases}$	$S_{\phi_{\text{ild}}} = \begin{cases} -j & (\text{CL}_{\text{anode}}) \\ +j & (\text{CL}_{\text{cathode}}) \end{cases}$	$S_{\phi_{\text{ild}}} = \begin{cases} -j & (\text{CL}_{\text{anode}}) \\ +j & (\text{CL}_{\text{cathode}}) \end{cases}$	$\text{A/m}^3$
ionic charge	$S_{\phi_i} = \begin{cases} -j & (\text{CL}_{\text{cathode}}) \\ +j & (\text{CL}_{\text{anode}}) \end{cases}$	$S_{\phi_i} = \begin{cases} -j & (\text{CL}_{\text{cathode}}) \\ +j & (\text{CL}_{\text{anode}}) \end{cases}$	$S_{\phi_i} = \begin{cases} -j & (\text{CL}_{\text{cathode}}) \\ +j & (\text{CL}_{\text{anode}}) \end{cases}$	$\text{A/m}^3$
energy	$S_T = S_Q + S_{rev} + S_{act} + S_{pc} + S_{pl}$	$S_T =  j  \left(  \eta  - \frac{T \Delta s}{nF} \right) + \frac{I^2}{K_m^{\text{eff}}} + S_{H_2O}^1 \Delta h_{fg}$	$S_T =  j  \left(  \eta  - \frac{T \Delta s}{nF} \right) + \frac{I^2}{K_m^{\text{eff}}} + S_{H_2O}^1 \Delta h_{fg}$	$\text{W/m}^3$

<sup>a</sup>From ref 35. <sup>b</sup>From ref 41. <sup>c</sup>From ref 61.

	one-dimensional model	two-dimensional model	three-dimensional model
transport mechanism	considers transport across the cell and neglects the variation across the surface of the cell	provides more detailed information compared to 1D, considering the transport in two planes, either along the channel or across the channel at a time	most detailed model among 1D and 2D, considering transport along the channels and across the channels simultaneously
accuracy	accuracy is less as a result of the assumption made to simplify the model to one-dimensional	more accurate compared to 1D	most accurate model
computational time required	less	medium	high
computational capacity required	less	medium	high

using cooling plates within stacks to avoid the rise in the temperature, which helps in avoiding dehydration of the membrane.

Liu et al.<sup>68</sup> used computational fluid cell dynamics (CFCD) to model a six cell mini PEM fuel stack using a 3D modeling approach for the first time. The simulation and experimental results were compared, and a close match was found between the results. The study found a relation between the temperature difference within the stack and the airflow rates. The results indicated that, at lower flow rates, the stack could not be cooled efficiently, which will increase the temperature of the stack.

Kvesić et al.<sup>69</sup> modeled a cell consisting of five cells with an active area of 200 cm<sup>2</sup>. The model predicted the highest value and the lowest value of the current density at the cathode inlet and cathode outlet, respectively. This study also indicated the importance of the cooling system in controlling the temperature of the stack. A single-phase 3D model was developed by Macedo-Valencia et al.<sup>70</sup> to analyze the five cell PEM fuel stack performance. The model results showed that the concentration of species was higher at the inlet and then gradually drops along the channel. The numerical modeling results were validated against the experimental results.

Mustata et al.<sup>71</sup> studied the airflow distribution in the PEM fuel cell stack for two different configurations, i.e., "U" shape and "Z" shape channel configurations. The pressure drop in both channel configurations was almost negligible. However, the results showed that the mass flow distribution was more uniform in the case of the "Z" channel configuration compared to the "U" channel configuration.

Chen et al.<sup>72</sup> developed a 2D model for a fuel stack consisting of 72 cells to investigate the pressure drop as a result of channel flow resistance, flow distribution, manifold widths, and air supply. A channel configuration with high channel resistance showed a more uniform flow distribution. The study also showed that a more uniform flow distribution can be gained with a low air supply than a higher air supply. Moreover, it was concluded that increasing the manifold width can help in achieving a high uniformly distributed flow and less pressure drop in the stack.

Zhang et al.<sup>73</sup> used a 3D model to examine a new cooling strategy applied to a five fuel cell stack. Chugh et al.<sup>74</sup> used a steady-state model to assess the influence of the operating parameters, pressure, temperature, stoichiometry, and relative humidity, of the inlet gases on the 30 cell PEM fuel cell stack performance. The results showed an increase in the cell performance with a rise in the pressure, relative humidity, and temperature. The results obtained from the simulation of the model were a good match with experimental data, with a 7–15% deviation with experimental results.

Like the single-cell models, 3D PEM fuel stack models are more realistic and accurate compared to 2D models but at the cost of higher computational cost and time. One of the major difficulties in the modeling and simulations of PEM fuel stacks is the higher computational time and cost. The geometry of the fuel stacks is many times bigger than the single cell, as a result of which the number of mesh grid elements increases substantially. The simulation of the PEM fuel cell stacks is hard without simplifications, and therefore, many researchers used simplified models for the simulation of the stack. For example, in the study conducted by Liu et al.,<sup>68</sup> the gas flow channels were simplified to be porous to reduce the number of mesh elements and, hence, reduce the computational time.

**Table 4.** Summary of Modeling of PEM Fuel Cell/Stacks from Reviewed Research Papers

reference	area of study	model dimension	data used for model validation
Springer et al. <sup>25</sup>	fuel cell performance	one-dimensional	experimental data
Bernardi and Verbrugge <sup>26</sup>	species transport mechanism and factors that influence fuel cell performance	one-dimensional	experimental data
Odetola et al. <sup>18</sup>	hydrogen consumption and water and thermal management	two-dimensional	none
Nguyen and White <sup>30</sup>	humidification effects	two-dimensional	none
Yi and Nguyen <sup>31</sup>	effect of different gas flow channel flow fields and operating conditions on the fuel cell performance	two-dimensional	none
Pasaogullari et al. <sup>37</sup>	transport of two phases within the PEM fuel cell	two-dimensional	none
Dutta and Shimpalee <sup>39</sup>	influence of heat generated on the PEM fuel cell performance	three-dimensional	none
Mazunder and Cole <sup>40</sup>	liquid water transport and formation	three-dimensional	experimental data
Berning and Djilali <sup>20</sup>	influence of the operating temperature and pressure on the performance of the PEM fuel cell	three-dimensional	experimental data
Ye and Nguyen <sup>41</sup>	formation of liquid water with GDLs and CLs of the PEM fuel cell	three-dimensional	none
Meng <sup>42</sup>	heat management issues by involving the process of condensation and evaporation	three-dimensional	none
Berning <sup>43</sup>	multiphase flow through the porous electrode	three-dimensional	none
Berning et al. <sup>45</sup>	liquid water flow from GDLs to the gas channels of the PEM fuel cell	three-dimensional	other publication results
Dawes et al. <sup>46</sup>	effect of water flooding on the PEM fuel cell performance	three-dimensional	other publication results
Yuan et al. <sup>47</sup>	influence of operating parameters, such as the pressure, cell temperature, air stoichiometric ratio, and relative humidity of reactants, on the PEM fuel cell performance	three-dimensional	experimental data
Li et al. <sup>55</sup>	influence of oxygen transport resistance and reduction of the catalyst on the PEM fuel cell performance at high current densities for an automotive	three-dimensional	none
Thosar et al. <sup>56</sup>	technique to find the <i>in situ</i> oxygen diffusion coefficients at different conditions	three-dimensional	experimental data
Wilberforce et al. <sup>57</sup>	explained some of the key design parameters of bipolar plate geometry, such as channel length, flow direction, and use of baffles, that can increase the PEM fuel cell performance	three-dimensional	none
Atyabi et al. <sup>58</sup>	assessing the influence of the pressure of cell assembly on the contact resistance between bipolar plates and GDL	three-dimensional	none
Carcadea et al. <sup>59</sup>	effects of the composition and properties of the catalyst layer, such as platinum loadings, particle radius ionomer, volume fraction, electrochemical active surface, and mass transport resistance from liquid water and ionomer covering particles of the catalyst, on the PEM fuel cell performance	three-dimensional	experimental data
Han and Chen <sup>60</sup>	studying the effects of the air velocity and wettability	two-dimensional	none
Wöhr et al. <sup>67</sup>	thermal and water management of single PEM fuel cell and multi-cell stacks (four single cells)	two-dimensional	none
Mustata et al. <sup>71</sup>	air flow distribution in the PEM fuel stack for two different configurations	three-dimensional	none
Macedo-Valencia et al. <sup>70</sup>	heat transfer, species transport, electrochemical reaction, and fluid flow in the PEM fuel cell stack (five single cells)	three-dimensional	experimental data
Kvesić et al. <sup>69</sup>	performance of multi-cell PEM stack (five single cells)	three-dimensional	local measurement of the temperature and current density
Mustata et al. <sup>71</sup>	air flow distribution in the PEM fuel stack for two different configurations	three-dimensional	none

Similarly, Chen et al.<sup>72</sup> used a simplified 2D model by ignoring the electrochemical reaction and heat and mass transport phenomena. Hence, such simplifications can be effective in reducing the computational cost and time, but at the same time, the accuracy of the results is compromised. Hence, balancing between accuracy and computational time is one of the main challenges for the researchers in the area of PEM stack simulation and modeling.

**2.6. Experimental Validation of the Models.** Validation is a critical step in CFD-based simulations of the fuel cells, in which the numerical simulation results are correlated with the experimental data.<sup>43</sup> Most of the researchers have validated their models by comparing the polarization curve of the simulation to that of the experimental data and, for various reasons, have found good agreement with some discrepancies.

Springer et al.<sup>25</sup> validated the predicted modeling results with experimental data at different operating conditions. Bernardi and Verbrugge<sup>26</sup> also verified the model results by comparing them to the experimental data by fitting the value of

exchange current density. Berning and Djilali<sup>20</sup> found a reasonable agreement between experimental and simulation results. Siegel et al.<sup>35</sup> also compared model results to the experimental results and found an excellent agreement. Liu et al.<sup>68</sup> also found a good match between simulation and experimental results. With Limjeerajarus and Charoenamornkitt,<sup>73</sup> a fair agreement was found between simulation and experimental results, with a minor discrepancy because of the existing exchange density assessment. The study conducted by Macedo-Valencia et al.<sup>70</sup> uses slightly different values from experimental data for the physical properties of membrane electrode assembly (MEA), which resulted in a discrepancy between the simulation and experimental data.

As a result of the unavailability of the precise and reliable data for different model input variables, such as charge transfer coefficients, open-cell voltage, exchange current densities, etc., the results obtained from the simulation are not very accurate.<sup>22</sup>

Harvey et al.<sup>44</sup> noted that catalyst agglomerate models are not included in the majority of CFD models that are used by researchers for the modeling of a fuel cell, as a result of which a sudden drop in the performance at higher currents caused by the mass transport losses are not observed. In the study conducted by Bernardi and Verbrugge,<sup>26</sup> the modeling simulation and experimental polarization curves were matched by tuning the values of the exchange current density; however, the exchange current density depends upon the temperature and Pt loading. Similarly, the model by Jung and Trung<sup>31</sup> was also unable to foresee a rapid drop in the voltage caused by concentration losses at high current densities, because the resistance to gases flowing through porous electrodes was not included in the model. The voltage value predicted by the model by Ferreira et al.<sup>50</sup> at 0.70 A/cm<sup>2</sup> was 15% higher than the voltage obtained experimentally. The possible reason for this variation in the voltage values is the application of the Leverett J-function at GDL for the calculation of the values of liquid saturation. Fuller and Newman<sup>76</sup> did not notice a sharp change in the polarization curve obtained from their model caused by mass transport losses before the current density exceeds 5 A/cm<sup>2</sup>, because the concentration losses resulting from the transport and adsorption of oxidants and reactants in water and ionomer film were not included in the model. The results obtained from the model by Mazumder and Cole<sup>77</sup> did not match the experimental results because of the insignificant factors, such as the dissolution of liquid species gases, Knudsen diffusion, obstruction of catalyst layer active sites by liquid water, etc. According to the results of modeling by Xing et al.<sup>78</sup> at high current densities, the resistance to oxygen diffusion through the water film increases, which causes a rapid decline in the performance. An agglomerate model by Moein-Jahromi and Kermani<sup>79</sup> was used to model the cathode catalyst layer, and then the simulation results were compared to the homogeneous cathode catalyst model. The homogeneous model results overpredicted the experimental results by 80%, while on the other hand, the agglomerate model results had a good match with the experimental data.

Some of the authors in the literature concluded that the models used for the simulation of the PEM fuel cell cannot be validated only by comparing the polarization curves obtained from experiments and simulation. The simulation results obtained from the model developed by Ju and Wang<sup>80</sup> had a reasonable agreement with experimental polarization curves, but at the current distribution level, the agreement was unsatisfactory, while the values of the model input parameters were the same. Lum and McGuirk<sup>81</sup> used experimental and simulated local current distribution data for their model validation. Because the collection of local distribution data for species gases and current density requires a highly sophisticated experimental setup, such as Mench et al.<sup>82</sup> used in their study, these data are generally unavailable. Therefore, this is one of the main reasons that most of the researchers in the literature assessed the accuracy of their models by just comparing the models and experimental polarization curves.<sup>53</sup>

As seen in Table 4, some of the authors did not validate their models experimentally in any way, while some authors, e.g., Bernardi et al.<sup>26</sup> and Siegel et al.,<sup>35</sup> matched their models and experimental polarization curves by varying the values of selected input model parameters that are not readily available or very hard to be measured experimentally. It remains a key limitation in fuel cell simulation modeling that values of model input parameters, such as exchange current density, charge

transfer coefficients, and other coefficients, are generally unavailable for a particular fuel cell and very hard if not impossible to measure independently by experiment.

### 3. PEM FUEL CELL MODELING SOFTWARE

Various specific commercial software, such as STAR-CD, ANSYS FLUENT, COMSOL, and OpenFOAM, were used to model and simulate fuel cells. The applications of these software to PEM fuel cell modeling have been recently reviewed by Kone et al.<sup>83</sup> Most of the software use the finite volume method (FVM) as a discretization technique for both the computational domain and partial differential equations, but there may be differences in the approach used for modeling of multiphase flow and phase change processes. These software have different appearances and modeling capabilities, but basically, all of them solve partial differential equations numerically with different multiphysics models or add-on fuel cell modules.<sup>83</sup> Table 5 compares the modeling capabilities and modeling approaches used by these software.

Moreover, the computational cost and time required for a CFD simulation software to give a converged solution depend upon a number of factors, such as the size of geometry (number of mesh elements), mesh quality (fine or coarse mesh), complexity of the problem (1D, 2D, 3D, single-phase, or multiphase), convergence criteria (values of parameters set for convergence criteria), and computing system capacity (RAM size, number of CPU cores, and series or parallel).

Imbrioscia and Fasoli<sup>85</sup> used OpenFOAM to predict the change in the behavior of the flow of gases as a result of the change in the geometry of bipolar plates and shape of flow fields. The purpose of this study was to predict the influence of the variation in channel width and shape over the flow of gases. Kone et al.<sup>86</sup> used OpenFOAM for the performance assessment of the PEM fuel cell.

Valiño et al.<sup>87</sup> studied the effects as a result of the change in the position of the inlet for the cathode and anode on the distribution of reactants inside the PEM fuel cell using OpenFOAM as a modeling tool. The findings of this study indicated that a large portion of the plate remains unused because most of the reactions occur near the inlet. As a result, the entry of gases can be clogged as a result of the excessive amount of water generation.

Haghayegh et al.<sup>88</sup> used COMSOL multiphysics to assess the PEM fuel cell performance with serpentine flow configuration. The model results showed a better performance for a catalyst with a high surface area and activated sites and, moreover, predicted reasonable reduction in the concentration of oxygen along the channel, which indicates the consumption of oxygen as a result of the electrochemical reaction. As a result of the higher oxygen consumption at the cathode, liquid water is produced at a higher rate.

Sezgin et al.<sup>89</sup> used COMSOL multiphysics for a high-temperature PEM fuel cell simulation to study the influence of membrane conductivity, inlet velocities of reactants, and design parameters on its performance.

Jourdani et al.<sup>90</sup> used COMSOL multiphysics to examine the influence of the membrane geometry on the PEM fuel cell performance. The study results showed that a PEM fuel cell with a thinner membrane produces a higher current, consumes more oxygen and hydrogen, and produces more water. The results of the simulation were compared to the experimental results, and good agreement was found.

**Table 5. Comparison of Different CFD Software Used for Simulation of PEM Fuel Cells<sup>83,84</sup>**

	ANSYS FLUENT	COMSOL	OpenFOAM	STAR-CD
modeling approach for multiphase flow	Eulerian–Eulerian and Eulerian–Lagrangian	bubbly flow, multiphase	two fluid phases, volume of fluid, multiphase mixture, and multi-fluid	Eulerian–multiphase mixture and Eulerian–Eulerian
graphic user interface (GUI)	simple to use	simple to use	no GUI	simple to use
personalization of the code	through UDFs using C++ or Python	through UDFs using Java or MATLAB	source codes can be modified directly using C++ or Python	custom programming can be imported as modules
solver stability	higher	medium	depends upon knowledge of the user	medium
programming skills	C++ and Python knowledge required for UDFs	Java and MATLAB knowledge required for UDFs	C++ and Python knowledge required to modify the source codes	Java
PEM fuel cell add-on module	yes	yes	no	yes
add-on module capabilities	electrochemistry, current and mass transport, heat source, transport, and liquid water formation	electrochemical phenomena in the electrodes, multiphase flows, and flow in porous media	no	electrochemistry and water management

Caglayan et al.<sup>10</sup> employed a non-isothermal 3D model and used COMSOL multiphysics to predict the current distribution over the membrane plus temperature and pressure distribution over the channels of the high-temperature PEM fuel cells.

Meng and Wang<sup>91</sup> used the user code capability of STAR-CD to implement the 3D electrochemical coupled transport model. The model results indicated that better performance can be obtained by adequately designing the low ranges of relative humidity. The model results predicted a better performance at a fully humidified anode but dry cathode and both low humidified inlets at a relative humidity of 26%.

Weng et al.<sup>92</sup> used CFD-ACE+ commercial CFD code to analyze and predict the current density distribution and concentration of reactants for different flow configurations and operating conditions.

Iranzo et al.<sup>23</sup> used ANSYS FLUENT software to predict the 50 cm<sup>2</sup> PEM fuel cell performance with two different flow configuration (parallel and serpentine) with experimental validation. Sierra et al.<sup>93</sup> applied ANSYS FLUENT commercial software to assess the PEM fuel cell performance for three different flow configurations: straight, serpentine, and interdigitated. Kahveci and Taymaz<sup>94</sup> used ANSYS FLUENT to analyze the effects of GDL porosity pressure and humidity of inlet gases on the PEM fuel cell performance. The experimental data and simulation results obtained were matched, and reasonable agreement was found.

#### 4. ANSYS FLUENT PEM FUEL CELL MODULE

As suggested by Wu,<sup>95</sup> there is a need of developing a comprehensive full cell transport model that has the capability of modeling the electric transport, chemistry, heat generation, water transport, and electrochemistry processes in the fuel cell with validation.

The ANSYS PEM fuel cell module is an add-on to the ANSYS FLUENT CFD software capable of modeling liquid water and transportation and formation, current and mass transportation, electrochemistry, and heat sources in PEM fuel cells.<sup>96</sup> Since its introduction, the module has undergone significant revisions. The ANSYS PEM fuel cell module was used as a submodule in the fuel cell and electrolysis add-on module until the release of ANSYS 17.0. In the ANSYS 17.0 and onward versions, a new fuel cell add-on module was added, called the PEM fuel cell module, with some new updates and added modeling capabilities compared to the old module (which are discussed below).<sup>96</sup>

The ANSYS PEM fuel cell module has been used by many researchers previously for the PEM fuel cell modeling. Maslan et al.<sup>97</sup> found the optimum porosity and polytetrafluoroethylene (PTFE) content in the GDLs of the PEM fuel cell while using this module. Ibrahimoglu et al.<sup>98</sup> investigated the influence of the spiral gas flow channel configuration on the PEM fuel cell performance. Zaman et al.<sup>99</sup> studied the effects of the channel flow field configuration on thermal distribution in the PEM fuel cell. Limjeerajarus and Charoen-amornkitt<sup>75</sup> used this add-on module to analyze the 5 cm<sup>2</sup> PEM fuel cell performance for six different gas flow channel configurations and different numbers of channels. Macedo-Valencia et al.<sup>70</sup> modeled the fuel cell stack using the ANSYS FLUENT fuel cell module. Bilgili and Siviroğlu<sup>100</sup> analyzed the influence of MEA thickness and operating pressure on the PEM fuel cell performance. Schwarz and Djilali<sup>101</sup> used this module to

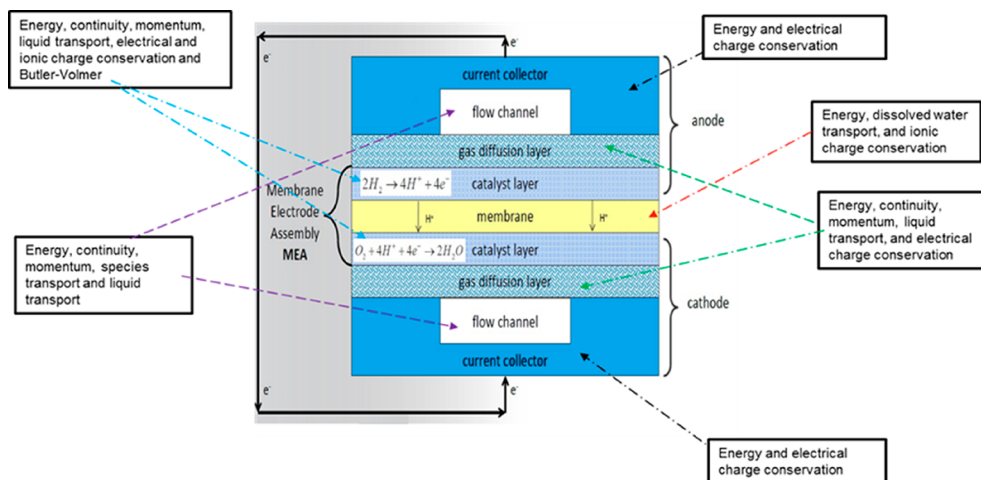


**Figure 8.** Illustration of the module governing equations on components of the PEM fuel cell.

model the cathode catalyst layer using a thin agglomerate model.

The ANSYS PEM fuel cell module has the full 3D modeling capability; therefore, it can give the best possible representation of all dimensions and properties of various components of a real fuel cell.<sup>102</sup> This module also has the capability of illustrating the realistic 3D geometry of stack, and the variation of the distribution of current and species across the individual cells of the stack. Moreover, the basic governing equations of the CFD and electrochemistry required solely for modeling the PEM fuel cell can be solved by FLUENT.

In version 17.0 and onward, of the ANSYS module have added a separate module for the PEM fuel cell with additional modeling capabilities compared to the earlier version.<sup>96</sup>

**Modeling anode and cathode microporous layers:** The microporous layer can minimize the contact resistance between the catalyst layer and GDLs to enhance the liquid water removal. The earlier version of the ANSYS PEM fuel cell module does not have the capability to model the microporous layers for the anode and cathode.

**Modeling transport for all three water phases (gas, liquid, and dissolved):** In the earlier PEM fuel cell module, water transport was modeled in two phases only, i.e., gas and liquid. The protons produced from the hydrogen oxidation reaction at the anode catalyst are dissolved in water, which results in the dissolved water phase. According to Kone et al.,<sup>83</sup> this phase of water was neglected by most of the researchers and was treated as a liquid phase.

**Solving liquid saturation in gas channels:** In the earlier version, the speed of liquid was assumed to be equivalent to the speed of gas in the channels (fine mist). While in the latest version, the water leaves GDLs in the liquid phase and enters gas flow channels. The main objective of modeling of liquid water in gas flow channels is to predict the increase in the pressure drop inside gas flow channels.

**Including of cathode agglomerate model:** In the latest version, ANSYS has modified the cathode catalyst model from the discrete volume model to the agglomerate model. The physical description of both models is the same, but the discrete volume model does not consider the transport of dissolved oxygen in the electrolyte phase as a result of the absence of agglomerate structures. The major concentration losses are caused by the transport of dissolved oxygen in the electrolyte phase.<sup>44</sup> As a result of the unavailability of an

agglomerate model, the old version was unable to capture the sharp drop in the voltage caused by concentration losses in the polarization curve at high current densities. With the inclusion of the agglomerate model in the latest version, now the sharp turn down in the polarization curve caused by mass transport constraints starts at relatively low current values compared to the older version.

On the basis of the modeling capabilities listed above and the comparison made in Table 5, it can be said that the ANSYS PEM fuel cell module in its current form has the capability of representing the phenomena taking place inside actual PEM fuel cells, in a more comprehensive way than other CFD software. A particular advantage of the ANSYS PEM fuel cell module is that the complex CFD and sophisticated electrostatic and electrochemical models are embodied in the module. Therefore, in the current paper, the ANSYS PEM fuel cell module is used as an example to understand the physical interpretation of the governing equations in terms of the practical processes taking place within PEM fuel cells, which will be helpful for the ANSYS PEM fuel cell module users.

The governing equations that are used by the ANSYS PEM fuel cell module for the modeling of PEM fuel cells are based on conservation of energy, conservation of mass, conservation of charge, conservation of momentum, and species transport. The following summary of the mathematical model has been taken from the current ANSYS PEM fuel cell module manual.<sup>96</sup> Figure 8 shows the module governing equations and their application on the components of the PEM fuel cell.

The driving force behind electrochemical reactions taking place in the anode and cathode catalysts is the difference in potential between the solid and membrane phases. Conservation of the charge equation is used to solve the electronic and protonic potentials

$$\nabla(\sigma_{\text{sol}} \nabla \phi_{\text{sol}}) + R_{\text{sol}} = 0 \quad (4)$$

$$\nabla(\sigma_{\text{mem}} \nabla \phi_{\text{mem}}) + R_{\text{mem}} = 0 \quad (5)$$

where  $\sigma$  is the electrical conductivity ( $\Omega^{-1} \text{ m}^{-1}$ ),  $\phi$  is the electric potential (V),  $R$  is the volumetric transfer current ( $\text{A}/\text{m}^3$ ), sol is the solid, and mem is the membrane.

Equation 4 is solved for electronic potential at electron-conducting solid regions, such as bipolar plates, GDLs, and catalyst layers, while eq 5 is solved for protonic potential at the membrane only.

The volumetric transfer current ( $R$ ) terms in eqs 4 and 5 are source terms, which are described by the Butler–Volmer equation as

$$R_{\text{an}} = (\zeta_{\text{an}} j_{\text{an}}(T)) \left( \frac{[A]}{[A]_{\text{ref}}} \right)^{\gamma_{\text{an}}} (-e^{+\alpha_{\text{an}}^{\text{an}} F \eta_{\text{an}} / RT} + e^{-\alpha_{\text{cat}}^{\text{an}} F \eta_{\text{an}} / RT}) \quad (6)$$

$$R_{\text{cat}} = (\zeta_{\text{cat}} j_{\text{cat}}(T)) \left( \frac{[C]}{[C]_{\text{ref}}} \right)^{\gamma_{\text{cat}}} (-e^{+\alpha_{\text{an}}^{\text{cat}} F \eta_{\text{cat}} / RT} + e^{-\alpha_{\text{cat}}^{\text{cat}} F \eta_{\text{cat}} / RT}) \quad (7)$$

where  $j_{\text{an/cat}}$  is the reference exchange current density per active surface area ( $\text{A}/\text{m}^2$ ),  $\zeta$  is the specific active surface area ( $\text{m}^{-1}$ ),  $[C]$  and  $[C]_{\text{ref}}$  are the local species concentration and reference value ( $\text{kmol}/\text{m}^3$ ), respectively,  $\gamma$  is the concentration-dependent exponent,  $\alpha_{\text{an}}^{\text{an}}$  and  $\alpha_{\text{cat}}^{\text{an}}$  are the anode and cathode transfer coefficients of the anode electrode, respectively,  $\alpha_{\text{an}}^{\text{cat}}$  and  $\alpha_{\text{cat}}^{\text{cat}}$  are the anode and cathode transfer coefficients of the cathode electrode, respectively,  $\eta_{\text{an}}$  and  $\eta_{\text{cat}}$  are the surface potentials for anode and cathode surfaces, respectively,  $R$  is the universal gas constant ( $8.314 \text{ J mol}^{-1} \text{ K}^{-1}$ ),  $T$  is the temperature (K), and  $F$  is the Faraday constant ( $9.65 \times 10^7 \text{ C/kmol}$ ).

Aside from Faraday and the universal gas constant, each of the above parameters are model input variables that can be tuned to obtain a better match between simulation and experimental results.

The amount of current generated is directly related to the specific active surface area  $\zeta$ , which can be reduced as a result of the catalyst flooding at high current densities. It is very complicated to calculate the exact numerical value for the specific active area; therefore, the value of this input parameter can be tuned to match simulated results with experimental results.

The values of both exchange current densities for the cathode and anode are tuned to match the simulated and experimental polarization curves, especially in the activation loss region of the polarization curve. Another important term is the concentration-dependent exponent. The default value is set to 1, but it can be varied.

The values of four different charge transfer coefficients are separately set as different input values. This emerged from the work undertaken by ref 102.

As a result of electrochemical reactions at catalyst layers, the reactants ( $\text{H}_2$ ) and oxidants ( $\text{O}_2$ ) are consumed, while water in the dissolved phase ( $\lambda$ ) is generated. The volumetric source terms ( $\text{kg m}^{-3} \text{ s}^{-1}$ ) for species and water in the dissolved phase are given by the conservation of mass

$$S_{\text{H}_2} = -\frac{M_{\text{w},\text{H}_2}}{2F} R_{\text{an}} < 0 \quad (8)$$

$$S_{\text{O}_2} = -\frac{M_{\text{w},\text{O}_2}}{4F} R_{\text{cat}} < 0 \quad (9)$$

$$S_{\lambda} = \frac{M_{\text{w},\text{H}_2\text{O}}}{2F} R_{\text{cat}} > 0 \quad (10)$$

where  $M_{\text{w},\text{H}_2\text{O}}$ ,  $M_{\text{w},\text{H}_2}$ , and  $M_{\text{w},\text{O}_2}$  are the molecular masses of water, hydrogen, and oxygen, respectively.

These equations relate the rate of consumption of reactants ( $\text{H}_2$ ) and oxidants ( $\text{O}_2$ ) to the current generated at the anode and cathode, respectively. The amount of current generated at the cathode is directly related to the rate of water generation,

which means that the chance of cathode flooding is higher at the higher current densities.

The total current produced at anode and cathode electrodes is the same, with the equation for the conservation of current given by

$$\int_{\text{an}} R_{\text{an}} \, dV = \int_{\text{cat}} R_{\text{cat}} \, dV \quad (11)$$

In a PEM fuel cell, the water exists in three different phases: dissolved water phase, liquid water phase, and water vapor phase. The mass transfer among these three phases may take place depending upon the thermodynamic conditions. Water is generated in the dissolved phase at the cathode catalyst layer as a result of the oxygen reduction reaction. On the basis of the local conditions, part of it is converted to either liquid water or water vapor. Because the PEM fuel cell operates at low temperatures (below 100 °C), at high current densities, water vapor may condense to liquid water as a result of condensation. This liquid water causes concentration losses as a result of blocking of pores and covering of catalyst active sites for reaction.

The water in the dissolved phase exists in the membrane and the ionomers of catalyst layers. The transport and generation of water in the dissolved phase is given by

$$\begin{aligned} \frac{\partial}{\partial t} (\varepsilon_i M_{\text{w},\text{H}_2\text{O}}) \frac{\rho_i}{EW} \lambda + \nabla \left( i_m \frac{n_d}{F} M_w \right) \\ = \nabla (M_w D_w^i \nabla \lambda) + S_{\lambda} + S_{\text{gd}} + S_{\text{ld}} \end{aligned} \quad (12)$$

where  $\varepsilon_i$  is the porosity of porous media,  $i_m$  is the ionic current density calculated as  $i_m = -\sigma_{\text{mem}} \nabla \phi_{\text{mem}}$ ,  $\lambda$  is the dissolved water content,  $n_d$  is the osmotic drag coefficient,  $D_w^i$  is the diffusion coefficient of the water content,  $S_{\lambda}$  is the water generation as a result of the oxygen reduction reaction at the cathode catalyst layer,  $S_{\text{gd}}$  is the rate of mass change between gas and the dissolved phase, and  $S_{\text{ld}}$  is the rate of mass change between liquid and the dissolved phase.

The liquid water generated is driven by the liquid pressure gradient ( $\nabla p_l$ ).<sup>96</sup> Transport of liquid water and water vapor are modeled by the following equations:

$$\frac{\partial (\varepsilon_i \rho_l s)}{\partial t} = \nabla \left( \frac{\rho_l K K_r}{\mu_1} \nabla p_l \right) + S_{\text{gl}} - S_{\text{ld}} \quad (13)$$

$$\nabla p_l = p_c + p \quad (14)$$

$$\frac{\partial (\varepsilon_i \rho_l s)}{\partial t} = \nabla \left( \frac{\rho_l K K_r}{\mu_1} \nabla (p_c + p) \right) + S_{\text{gl}} - S_{\text{ld}} \quad (15)$$

where  $\rho_l$  is the liquid water density,  $\mu_1$  is the liquid dynamic viscosity,  $K$  is the absolute permeability,  $K_r$  is the relative permeability, and  $S_{\text{gl}}$  is the rate of mass transfer between gas and liquid phases

$$\frac{\partial (\varepsilon_i \rho_l s)}{\partial t} = \nabla \left( \frac{\rho_l K K_r}{\mu_1} \nabla (p_c + p) \right) + S_{\text{gl}} - S_{\text{ld}} \quad (16)$$

The first term on the right-hand side of eq 16 is called capillary diffusion flux ( $j_l$ ), which transports liquid water from a higher liquid saturation region to a lower region by capillary force.

$$j_1 = \left( \frac{\rho_1 K K_r}{\mu_1} \nabla (p_c + p) \right) \quad (17)$$

The capillary pressure “ $p_c$ ” is defined by<sup>96</sup>

$$p_c = \sigma \cos \theta_c \sqrt{\frac{\epsilon}{K}} J(1-s); \quad \text{if } \theta_c < 90^\circ \quad (18)$$

$$p_c = \sigma \cos \theta_c \sqrt{\frac{\epsilon}{K}} J(s); \quad \text{if } \theta_c > 90^\circ \quad (19)$$

where  $\theta_c$  is the contact angle inside the pores of the GDL and  $\sigma$  is the surface tension.

Because of the absence of the methods for estimating the contact angle inside the small pores of the GDL, it is commonly assumed that the external contact angle is the same as the internal pore contact angle.<sup>103</sup> Therefore, in the simulation, the value of the internal pore contact angle can be assumed to be the same as on the external surface that is measured by a sessile drop method.<sup>104</sup>

The value of capillary pressure for contact angles within the hydrophobic range, i.e., contact angle,  $\theta_c$ , of  $>90^\circ$ , is given by eq 19 in the module.<sup>96</sup>

With the increase of the value of the contact angle within the hydrophobic range, the value of capillary pressure will be increased. Variation in the values of the contact angle input to the simulation, therefore, has a direct influence on the capillary pressure (eqs 18 and 19), which is the main driving force in removing water from the cell (eq 20).

The capillary pressure extracts liquid water produced at the cathode electrode as a result of the electrochemical reaction out of the GDL to gas flow channels.<sup>96</sup> It can be seen from eq 20 that the liquid water flux out of GDL into channels is directly related to the capillary pressure and porosity.<sup>96</sup> Increasing each of these factors will thus enhance the liquid water removal out of the cell

$$f_{\text{liq}} = \Theta \epsilon s \max \left[ \left( p_c + \frac{1}{2} \rho V^2 \right), 0 \right] \quad (20)$$

where  $\Theta$  is the liquid removal coefficient and  $\rho V^2$  is the local dynamic head in the gas flow channels.

On the basis of the local thermodynamic conditions, the liquid water and water vapor may change to one another phases through condensation and evaporation. The condensation and evaporation processes taking place inside the PEM fuel cell are described by

$$S_{\text{gl}} = \gamma_e \epsilon s D_{\text{gl}} \frac{M_{\text{w}, \text{H}_2\text{O}}}{RT} p \ln \left( \frac{p - p_{\text{sat}}}{p - p_{\text{ww}}} \right), \quad p_{\text{ww}} \leq p_{\text{vv}} \\ (\text{evaporation}) \quad (21)$$

$$S_{\text{gl}} = \gamma_c \epsilon (1 - s) D_{\text{gl}} \frac{M_{\text{w}, \text{H}_2\text{O}}}{RT} p \ln \left( \frac{p - p_{\text{sat}}}{p - p_{\text{ww}}} \right), \quad p_{\text{vv}} > p_{\text{ww}} \\ (\text{condensation}) \quad (22)$$

where  $\gamma_e$  and  $\gamma_c$  are the evaporation rate coefficient and condensation rate coefficient, respectively.

The term “ $s$ ” refers to liquid water saturation, which is an important factor for the concentration loss modeling in the PEM fuel cell. The value of this output parameter indicates

how much active surface area has been flooded and how much species flow is constrained by liquid water.

At higher current densities, these concentration losses become more dominant in the PEM fuel cells and, hence, unitized regenerative fuel cells (URFCs) in the fuel cell mode. The mass transport losses are due to the following three main reasons.

**Mass Transport Losses as a Result of the Resistance by the Catalyst Microstructure.** The resistance caused by the catalyst to the transport of oxygen also contributes to the mass transport losses in the PEM fuel cell, which are not included in eq 7. These losses can be due to two factors: resistance as a result of the ionomer film,  $R_{\text{ion}}$ , and resistance caused by the liquid water film covering catalyst particles,  $R_{\text{liq}}$ .

The volumetric current transfer inside cathode layers after including these resistances is given by

$$R_{\text{cat}} = 4F \frac{C_{\text{O}_2}}{C_{\text{O}_2}/J_{\text{O}_2}^{\text{ideal}} + R_{\text{ion}} + R_{\text{liq}}} \quad (23)$$

where  $C_{\text{O}_2}$  is the concentration of oxygen

$$R_{\text{liq}} = \frac{\zeta_{\text{cat}} r_p^2}{K_w D_w} \frac{\left( \sqrt[3]{1 + \frac{s\epsilon}{1-\epsilon}} \right) - 1}{3(1-\epsilon)} \quad (24)$$

where  $\zeta_{\text{cat}}$  is the specific active surface area of the cathode catalyst ( $\text{m}^{-1}$ ),  $\epsilon$  is the porosity,  $r_p$  is the particle diameter,  $K_w D_w$  is the product of diffusivity in liquid water and oxygen solubility

$$J_{\text{O}_2}^{\text{ideal}} = \frac{R_{\text{cat}}^0}{4F} \quad (25)$$

where  $R_{\text{cat}}^0$  is the the ideal transfer current from eq 7.

The values for parameters such as  $R_{\text{ion}}$ ,  $\zeta_{\text{cat}}$ ,  $r_p$ , and  $K_w D_w$  can be varied to obtain a good fit for the concentration polarization region of the polarization curve with experimental results.

**Mass Transport Losses as a Result of Water Flooding of Catalyst Active Sites.** The second critical factor that contributes to mass transport losses is the flooding of active catalyst sites that reduce the effective active surface area in the catalyst layers. The flooding of the catalyst reduces the current density by

$$R_j = (1 - s)^{\gamma_j} R_{\text{cat}}^0 \quad (26)$$

where  $\gamma_j$  is the user-specified constant.

The power  $\gamma_j$  shows the intensity of water flooding; this is also an input parameter that can be varied to obtain a good fit for the concentration polarization region of the polarization curve with experimental results.

**Mass Transport Losses as a Result of Blockage of Pores.** Liquid water may also block the pores of GDLs and the catalyst, which affects the diffusivity of species by

$$D_{\text{eff}}^{ij} = (1 - s)^{r_s} \epsilon^{1.5} D^{ij} \quad (27)$$

The term  $(1 - s)^{r_s}$  represents the blockage of GDL pores as a result of liquid water.

$r_s$  is called the exponent of pore blockage, which can be tuned to obtain a good fit in the mass transport loss region of the simulated polarization curve with experimental results.

## 5. GAPS IDENTIFIED IN THE CURRENT KNOWLEDGE OF PEM FUEL CELL MODELING

From the foregoing review, the gaps in knowledge and future recommendation relating to the simulation modeling of PEM fuel cells emerge as follows: (1) There is a lack of clear understanding to model the much rapid voltage drop at higher current densities as a result of concentration losses. These concentration losses are due to several factors: flooding of active sites of catalysts, blocking of pores of catalyst layers and GDLs by water, and resistance to the flow of oxygen as a result of the ionomer covering catalyst particles. Different researchers could not predict the steep turn down in the concentration polarization region as a result of a number of reasons.<sup>44,26,76,31,77–79</sup> However, the current versions of the ANSYS module are considering the concentration losses because of the resistance to the flow of oxygen as a result of the ionomer covering catalyst particles. Hence, we are obtaining the sharp drop at relatively low current densities compared to the earlier version of simulation results. (2) Most of the researchers have matched their simulated results with experimental data without following a systematic procedure, which is very time-consuming. Thus, there is a lack of a step-by-step procedure to match an experimental polarization curve with a simulated polarization curve. A systematic procedure for matching the simulated and experimental polarization curves is developed in our previous study.<sup>105</sup> (3) Most of the researchers have compared the results of their model to one set of the experimental results. To reduce the probability of error between simulation and experimental results, the simulated results should be compared at least with two sets of experimental data at different operating conditions. The studies conducted by refs 105–107 compared the results of simulation to two sets of experimental data operating at different operating conditions. (4) Most of the papers have focused on studying the influence of different parameters (e.g., catalyst properties, membrane conductivities, wettability of GDL, channel configurations, operating conditions, etc.) on the performance of PEM fuel cells. Some of the studies, such as refs 108–111, have diagnosed the performance of the PEM fuel cells, but this diagnostic analysis was not based on the CFD simulation and modeling techniques. (5) Most of the research papers in the literature review are focused on the dedicated modeling of a single PEM fuel cell, and the work performed on the modeling of URFCs is extremely limited. Doddathimmaiah and Andrews<sup>112</sup> used the theoretical relationship to develop a computer model that was used to study the influence of main variables, such as charge transfer coefficients and exchange current densities, on the performance of the single URFC in the fuel cell and electrolyzer mode. Guarneri et al.<sup>113</sup> developed a zero-dimensional steady-state model to investigate the performance of PEM URFC in fuel cell mode. (6) The application of artificial intelligence is very crucial for the energy sector and research for the redesigning of the energy systems.<sup>114</sup> Artificial intelligence can also be helpful in the modeling and simulations of the PEM fuel cells. For example, for a single voltage/current density point, the simulation to reach a converged solution takes a long time, and to plot a whole polarization curve from the simulation data, the computational time multiplies. An algorithm can be developed and incorporated to the simulation codes, which then automatically and systematically matches simulated and experimental polarization curves, in terms of reducing the

percentage difference between simulated and experimental results.

## ■ AUTHOR INFORMATION

### Corresponding Author

Muhammad Arif – School of Engineering, RMIT University, Bundoora, Victoria 3083, Australia;  [orcid.org/0000-0002-5122-9863](https://orcid.org/0000-0002-5122-9863); Email: [muhammad.arif@student.rmit.edu.au](mailto:muhammad.arif@student.rmit.edu.au)

### Authors

Sherman C. P. Cheung – School of Engineering, RMIT University, Bundoora, Victoria 3083, Australia

John Andrews – School of Engineering, RMIT University, Bundoora, Victoria 3083, Australia

Complete contact information is available at:  
<https://pubs.acs.org/10.1021/acs.energyfuels.0c02414>

### Notes

The authors declare no competing financial interest.

## ■ NOMENCLATURE

$u$  = velocity (m/s)

$S$  = source term

$P$  = pressure (Pa)

$H_2$  = hydrogen

$O_2$  = oxygen

$D$  = diffusivity

$s$  = liquid saturation

$K$  = permeability ( $m^2$ )

$j$  = volumetric reaction rate ( $A/m^3$ )

### Greek Symbols

$\rho$  = density ( $kg/m^3$ )

$\mu$  = dynamic viscosity ( $kg\ m^{-1}\ s^{-1}$ )

$\phi$  = electrical potential (V)

$\sigma$  = electrical conductivity (S/m)

### Superscripts and Subscripts

$m$  = mass

$g$  = gas phase

$l$  = liquid phase

$wv$  = water vapor

$WD$  = water dissolved

$sld$  = electronic

$i$  = ionic

## ■ REFERENCES

- (1) Strachan, N.; Foxon, T. I. M.; Fujino, J. Policy implications from the Low-Carbon Society (LCS) modelling project. *Climate Policy* **2008**, *8* (sup1), S17–S29.
- (2) Luo, X.; Wang, J.; Dooner, M.; Clarke, J. Overview of current development in electrical energy storage technologies and the application potential in power system operation. *Appl. Energy* **2015**, *137*, 511–536.
- (3) Chen, H.; Cong, T. N.; Yang, W.; Tan, C.; Li, Y.; Ding, Y. Progress in electrical energy storage system: A critical review. *Prog. Nat. Sci.* **2009**, *19* (3), 291–312.
- (4) Preuster, P.; Alekseev, A.; Wasserscheid, P. Hydrogen Storage Technologies for Future Energy Systems. *Annu. Rev. Chem. Biomol. Eng.* **2017**, *8* (1), 445–471.
- (5) Dihrab, S. S.; Sopian, K.; Alghoul, M. A.; Sulaiman, M. Y. Review of the membrane and bipolar plates materials for conventional and unitized regenerative fuel cells. *Renewable Sustainable Energy Rev.* **2009**, *13* (6–7), 1663–1668.
- (6) Oberoi, A. S. Reversible Electrochemical Storage of Hydrogen in Activated Carbons from Victorian Brown Coal and Other Precursors.

- Ph.D. Thesis, School of Aerospace Mechanical and Manufacturing Engineering, RMIT University, Melbourne, Victoria, Australia, 2015; DOI: 10.13140/RG.2.2.32654.15686.
- (7) Barbir, F. *PEM Fuel Cells: Theory and Practice*, 2nd ed.; Academic Press: Waltham, MA, 2013; DOI: 10.1016/C2011-0-06706-6.
- (8) Wang, Y.; Chen, K. S.; Mishler, J.; Cho, S. C.; Adroher, X. C. A review of polymer electrolyte membrane fuel cells: Technology, applications, and needs on fundamental research. *Appl. Energy* **2011**, *88* (4), 981–1007.
- (9) Wu, H. Mathematical Modeling of Transient Transport Phenomena in PEM Fuel Cells. Ph.D. Thesis, University of Waterloo, Waterloo, Ontario, Canada, 2009.
- (10) Caglayan, D. G.; Sezgin, B.; Devrim, Y.; Eroglu, I. Three-dimensional non-isothermal model development of high temperature PEM fuel cells. *Int. J. Hydrogen Energy* **2018**, *43* (23), 10834–10841.
- (11) Wang, Y.; Leung, D. Y. C.; Xuan, J.; Wang, H. A review on unitized regenerative fuel cell technologies, part-A: Unitized regenerative proton exchange membrane fuel cells. *Renewable Sustainable Energy Rev.* **2016**, *65*, 961–977.
- (12) Rowe, A.; Li, X. Mathematical modeling of proton exchange membrane fuel cells. *J. Power Sources* **2001**, *102* (1), 82–96.
- (13) Boettner, D. D.; Paganelli, G.; Guezennec, Y. G.; Rizzoni, G.; Moran, M. J. Proton Exchange Membrane Fuel Cell System Model for Automotive Vehicle Simulation and Control. *J. Energy Resour. Technol.* **2002**, *124* (1), 20–27.
- (14) Kumar, A.; Reddy, R. G. Materials and design development for bipolar/end plates in fuel cells. *J. Power Sources* **2004**, *129* (1), 62–67.
- (15) Asghari, S.; Shahsmandi, M. H.; Ashraf Khorasani, M. R. Design and manufacturing of end plates of a 5 kW PEM fuel cell. *Int. J. Hydrogen Energy* **2010**, *35* (17), 9291–9297.
- (16) Park, S.; Lee, J.-W.; Popov, B. N. A review of gas diffusion layer in PEM fuel cells: Materials and designs. *Int. J. Hydrogen Energy* **2012**, *37* (7), 5850–5865.
- (17) Wu, B.; Zhao, M.; Shi, W.; Liu, W.; Liu, J.; Xing, D.; Yao, Y.; Hou, Z.; Ming, P.; Gu, J.; Zou, Z. The degradation study of Nafion/PTFE composite membrane in PEM fuel cell under accelerated stress tests. *Int. J. Hydrogen Energy* **2014**, *39* (26), 14381–14390.
- (18) Odetola, P.; Popoola, P.; Popoola, O.; Delport, D. Electro-deposition of Functional Coatings on Bipolar Plates for Fuel Cell Applications—A Review. In *Electrodeposition of Composite Materials*; Mohamed, A. M. A., Golden, T. D., Eds.; IntechOpen Limited: London, U.K., 2016; DOI: 10.5772/62169.
- (19) Li, C.; Liu, Y.; Xu, B.; Ma, Z. *Processes* **2019**, *7* (7), 419.
- (20) Berning, T.; Djilali, N. Three-dimensional computational analysis of transport phenomena in a PEM fuel cell—A parametric study. *J. Power Sources* **2003**, *124* (2), 440–452.
- (21) Hosseinzadeh, E. Modeling and Design of Hybrid PEM Fuel Cell Systems for Lift Trucks. Ph.D. Thesis, Department of Mechanical Engineering, Technical University of Denmark, Kongens Lyngby, Denmark, 2012.
- (22) Bednarek, T.; Tsotridis, G. Issues associated with modelling of proton exchange membrane fuel cell by computational fluid dynamics. *J. Power Sources* **2017**, *343*, 550–563.
- (23) Iranzo, A.; Muñoz, M.; Rosa, F.; Pino, J. Numerical model for the performance prediction of a PEM fuel cell. Model results and experimental validation. *Int. J. Hydrogen Energy* **2010**, *35* (20), 11533–11550.
- (24) Berning, T.; Djilali, N. Three-dimensional computational analysis of transport phenomena in a PEM fuel cell - A parametric study. *J. Power Sources* **2003**, *124* (2), 440–452.
- (25) Springer, T. E.; Zawodzinski, T. A.; Gottesfeld, S. Polymer Electrolyte Fuel Cell Model. *J. Electrochem. Soc.* **1991**, *138* (8), 2334–2342.
- (26) Bernardi, D. M.; Verbrugge, M. W. A mathematical model of the solid-polymer-electrolyte fuel cell. *J. Electrochem. Soc.* **1992**, *139* (9), 2477–2491.
- (27) Pasaogullari, U.; Wang, C. Y. *J. Electrochem. Soc.* **2004**, *151* (3), A399–A406.
- (28) Rahman, M. A.; Mojica, F.; Sarker, M.; Chuang, P.-Y. A. Development of 1-D multiphysics PEMFC model with dry limiting current experimental validation. *Electrochim. Acta* **2019**, *320*, 134601.
- (29) Ionescu, V. Water and hydrogen transport modelling through the membrane-electrode assembly of a PEM fuel cell. *Phys. Scr.* **2020**, *95* (3), 034006.
- (30) Nguyen, T. V.; White, R. E. A Water and Heat Management Model for Proton-Exchange-Membrane Fuel Cells. *J. Electrochem. Soc.* **1993**, *140* (8), 2178–2186.
- (31) Yi, J. S.; Nguyen, T. V. An Along-the-Channel Model for Proton Exchange Membrane Fuel Cells. *J. Electrochem. Soc.* **1998**, *145* (4), 1149–1159.
- (32) Chu, H.-S.; Yeh, C.; Chen, F. Effects of porosity change of gas diffuser on performance of proton exchange membrane fuel cell. *J. Power Sources* **2003**, *123* (1), 1–9.
- (33) Abdollahzadeh, M.; Pascoa, J. C.; Ranjbar, A. A.; Esmaili, Q. Analysis of PEM (Polymer Electrolyte Membrane) fuel cell cathode two-dimensional modeling. *Energy* **2014**, *68*, 478–494.
- (34) Marr, C.; Li, X. Composition and performance modelling of catalyst layer in a proton exchange membrane fuel cell. *J. Power Sources* **1999**, *77* (1), 17–27.
- (35) Siegel, N. P.; Ellis, M. W.; Nelson, D. J.; von Spakovsky, M. R. A two-dimensional computational model of a PEMFC with liquid water transport. *J. Power Sources* **2004**, *128* (2), 173–184.
- (36) Weber, A. Z.; Darling, R. M.; Newman, J. Modeling two-phase behavior in PEFCs. *J. Electrochem. Soc.* **2004**, *151*, A1715.
- (37) Pasaogullari, U.; Wang, C.-Y.; Chen, K. S. Two-Phase Transport in Polymer Electrolyte Fuel Cells with Bilayer Cathode Gas Diffusion Media. *J. Electrochem. Soc.* **2005**, *152* (8), A1574–A1582.
- (38) Fontana, É.; Mancusi, E.; Ulson de Souza, A. A.; Guelli Ulson de Souza, S. M. A. Flow regimes for liquid water transport in a tapered flow channel of proton exchange membrane fuel cells (PEMFCs). *J. Power Sources* **2013**, *234*, 260–271.
- (39) Dutta, S.; Shimpalee, S. Numerical Prediction of Temperature Distribution in PEM Fuel Cells. *Numer. Heat Transfer, Part A* **2000**, *38* (2), 111–128.
- (40) Mazumder, S.; Cole, J. V. Rigorous 3-D Mathematical Modeling of PEM Fuel Cells. *J. Electrochem. Soc.* **2003**, *150* (11), A1503.
- (41) Ye, Q.; Nguyen, T. V. Three-Dimensional Simulation of Liquid Water Distribution in a PEMFC with Experimentally Measured Capillary Functions. *J. Electrochem. Soc.* **2007**, *154* (12), B1242–B1251.
- (42) Meng, H. A two-phase non-isothermal mixed-domain PEM fuel cell model and its application to two-dimensional simulations. *J. Power Sources* **2007**, *168* (1), 218–228.
- (43) Berning, T. A Three-dimensional, Two-fluid Model of PEM Fuel Cell Cathodes. *ECS Transactions* **2009**, *16* (2), 23–34.
- (44) Harvey, D.; Pharoah, J. G.; Karan, K. A comparison of different approaches to modelling the PEMFC catalyst layer. *J. Power Sources* **2008**, *179* (1), 209–219.
- (45) Berning, T.; Odgaard, M.; Kær, S. K. A Computational Analysis of Multiphase Flow Through PEMFC Cathode Porous Media Using the Multifluid Approach. *J. Electrochem. Soc.* **2009**, *156* (11), B1301–B1311.
- (46) Dawes, J. E.; Hanspal, N. S.; Family, O. A.; Turan, A. Three-dimensional CFD modelling of PEM fuel cells: An investigation into the effects of water flooding. *Chem. Eng. Sci.* **2009**, *64* (12), 2781–2794.
- (47) Yuan, W.; Tang, Y.; Pan, M.; Li, Z.; Tang, B. Model prediction of effects of operating parameters on proton exchange membrane fuel cell performance. *Renewable Energy* **2010**, *35* (3), 656–666.
- (48) Golpaygan, A.; Sarchami, A.; Ashgriz, N. *Int. J. Energy Res.* **2011**, *35* (13), 1188–1199.
- (49) Inamuddin; Cheema, T. A.; Zaidi, S. M. J.; Rahman, S. U. Three dimensional numerical investigations for the effects of gas diffusion layer on PEM fuel cell performance. *Renewable Energy* **2011**, *36* (2), 529–535.

- (50) Ferreira, R. B.; Falcão, D. S.; Oliveira, V. B.; Pinto, A. M. F. R. 1D + 3D two-phase flow numerical model of a proton exchange membrane fuel cell. *Appl. Energy* **2017**, *203*, 474–495.
- (51) Ashrafi, M.; Shams, M. The effects of flow-field orientation on water management in PEM fuel cells with serpentine channels. *Appl. Energy* **2017**, *208*, 1083–1096.
- (52) Zhang, G.; Jiao, K. Three-dimensional multi-phase simulation of PEMFC at high current density utilizing Eulerian-Eulerian model and two-fluid model. *Energy Convers. Manage.* **2018**, *176*, 409–421.
- (53) Li, S.; Sundén, B. Effects of gas diffusion layer deformation on the transport phenomena and performance of PEM fuel cells with interdigitated flow fields. *Int. J. Hydrogen Energy* **2018**, *43* (33), 16279–16292.
- (54) Havaej, P.; Kermani, M. J.; Abdollahzadeh, M.; Heidary, H.; Moradi, A. A numerical modeling study on the influence of catalyst loading distribution on the performance of polymer electrolyte membrane fuel cell. *Int. J. Hydrogen Energy* **2018**, *43* (21), 10031–10047.
- (55) Li, Y.; Zhou, Z.; Liu, X.; Wu, W.-T. Modeling of PEM fuel cell with thin MEA under low humidity operating condition. *Appl. Energy* **2019**, *242*, 1513–1527.
- (56) Thosar, A. U.; Agarwal, H.; Govarthan, S.; Lele, A. K. Comprehensive analytical model for polarization curve of a PEM fuel cell and experimental validation. *Chem. Eng. Sci.* **2019**, *206*, 96–117.
- (57) Wilberforce, T.; El Hassan, Z.; Ogungbemi, E.; Ijaodola, O.; Khatib, F. N.; Durrant, A.; Thompson, J.; Baroutaji, A.; Olabi, A. G. A comprehensive study of the effect of bipolar plate (BP) geometry design on the performance of proton exchange membrane (PEM) fuel cells. *Renewable Sustainable Energy Rev.* **2019**, *111*, 236–260.
- (58) Atyabi, S. A.; Afshari, E.; Wongwises, S.; Yan, W.-M.; Hadjadj, A.; Shadloo, M. S. Effects of assembly pressure on PEM fuel cell performance by taking into accounts electrical and thermal contact resistances. *Energy* **2019**, *179*, 490–501.
- (59) Carcdea, E.; Varlam, M.; Marinoiu, A.; Raceanu, M.; Ismail, M. S.; Ingham, D. B. Influence of catalyst structure on PEM fuel cell performance—A numerical investigation. *Int. J. Hydrogen Energy* **2019**, *44* (25), 12829–12841.
- (60) Han, C.; Chen, Z. Numerical simulations of two-phase flow in a proton-exchange membrane fuel cell based on the generalized design method. *Energy Sources, Part A* **2019**, *41* (10), 1253–1271.
- (61) Havaej, P. A numerical investigation of the performance of Polymer Electrolyte Membrane fuel cell with the converging-diverging flow field using two-phase flow modeling. *Energy* **2019**, *182*, 656–672.
- (62) Li, Y.; Zhou, Z.; Liu, X.; Wu, W.-T. Modeling of PEM fuel cell with thin MEA under low humidity operating condition. *Appl. Energy* **2019**, *242*, 1513–1527.
- (63) Xie, B.; Jiang, Y.; Zhang, G.; Yin, Y.; Du, Q.; Jiao, K. Large-Scale Simulation of PEM Fuel Cell Using a “3D+1D” Model. *SAE Tech. Pap. Ser.* **2020**, DOI: [10.4271/2020-01-0860](https://doi.org/10.4271/2020-01-0860).
- (64) Zhang, G.; Wu, J.; Wang, Y.; Yin, Y.; Jiao, K. Investigation of current density spatial distribution in PEM fuel cells using a comprehensively validated multi-phase non-isothermal model. *Int. J. Heat Mass Transfer* **2020**, *150*, 119294.
- (65) Shan, Y. Dynamic Modeling of Polymer Electrolyte Membrane Fuel Cell Stack with 1D and 2D CFD Techniques. M.S. Thesis, Auburn University, Auburn, AL, 2006.
- (66) Gao, F.; Blunier, B.; Miraoui, A.; El Moudni, A. A Multiphysics Dynamic 1-D Model of a Proton-Exchange-Membrane Fuel-Cell Stack for Real-Time Simulation. *IEEE Trans. Ind. Electron.* **2010**, *57* (6), 1853–1864.
- (67) Wöhr, M.; Bolwin, K.; Schnurnberger, W.; Fischer, M.; Neubrand, W.; Eigenberger, G. Dynamic modelling and simulation of a polymer membrane fuel cell including mass transport limitation. *Int. J. Hydrogen Energy* **1998**, *23* (3), 213–218.
- (68) Liu, Z.; Mao, Z.; Wang, C.; Zhuge, W.; Zhang, Y. Numerical simulation of a mini PEMFC stack. *J. Power Sources* **2006**, *160* (2), 1111–1121.
- (69) Kvesić, M.; Reimer, U.; Froning, D.; Lüke, L.; Lehnert, W.; Stoltzen, D. 3D modeling of a 200 cm<sup>2</sup> HT-PEFC short stack. *Int. J. Hydrogen Energy* **2012**, *37* (3), 2430–2439.
- (70) Macedo-Valecia, J.; Sierra, J. M.; Figueroa-Ramirez, S. J.; Diaz, S. E.; Meza, M. 3D CFD modeling of a PEM fuel cell stack. *Int. J. Hydrogen Energy* **2016**, *41* (48), 23425–23433.
- (71) Mustata, R.; Valiño, L.; Barreras, F.; Gil, M. I.; Lozano, A. Study of the distribution of air flow in a proton exchange membrane fuel cell stack. *J. Power Sources* **2009**, *192* (1), 185–189.
- (72) Chen, C.-H.; Jung, S.-P.; Yen, S.-C. Flow distribution in the manifold of PEM fuel cell stack. *J. Power Sources* **2007**, *173* (1), 249–263.
- (73) Zhang, G.; Yuan, H.; Wang, Y.; Jiao, K. Three-dimensional simulation of a new cooling strategy for proton exchange membrane fuel cell stack using a non-isothermal multiphase model. *Appl. Energy* **2019**, *255*, 113865.
- (74) Chugh, S.; Chaudhari, C.; Sonkar, K.; Sharma, A.; Kapur, G. S.; Ramakumar, S. S. V. Experimental and modelling studies of low temperature PEMFC performance. *Int. J. Hydrogen Energy* **2020**, *45* (15), 8866–8874.
- (75) Limjeerajarus, N.; Charoen-amornkitt, P. Effect of different flow field designs and number of channels on performance of a small PEFC. *Int. J. Hydrogen Energy* **2015**, *40* (22), 7144–7158.
- (76) Fuller, T. F.; Newman, J. Water and Thermal Management in Solid-Polymer-Electrolyte Fuel Cells. *J. Electrochem. Soc.* **1993**, *140* (5), 1218–1225.
- (77) Mazumder, S.; Cole, J. V. Rigorous 3-D Mathematical Modeling of PEM Fuel Cells - II. Model Predictions with Liquid Water Transport. *J. Electrochem. Soc.* **2003**, *150* (11), A1510–A1517.
- (78) Xing, L.; Mamlouk, M.; Scott, K. A two dimensional agglomerate model for a proton exchange membrane fuel cell. *Energy* **2013**, *61*, 196–210.
- (79) Moein-Jahromi, M.; Kermani, M. J. Performance prediction of PEM fuel cell cathode catalyst layer using agglomerate model. *Int. J. Hydrogen Energy* **2012**, *37* (23), 17954–17966.
- (80) Ju, H.; Wang, C.-Y. *J. Electrochem. Soc.* **2004**, *151* (11), A1954–A1960.
- (81) Lum, K. W.; McGuirk, J. J. Three-dimensional model of a complete polymer electrolyte membrane fuel cell – model formulation, validation and parametric studies. *J. Power Sources* **2005**, *143* (1), 103–124.
- (82) Mench, M. M.; Wang, C. Y.; Ishikawa, M. *J. Electrochem. Soc.* **2003**, *150* (8), A1052–A1059.
- (83) Kone, J.-P.; Zhang, X.; Yan, Y.; Hu, G.; Ahmadi, G. Three-dimensional multiphase flow computational fluid dynamics models for proton exchange membrane fuel cell: A theoretical development. *J. Comput. Multiphase Flows* **2017**, *9* (1), 3–25.
- (84) Legendre, D. *CFD Software Overview Comparison, Limitations and User Interfaces*, 2015; <https://docplayer.net/3117668-Cfd-software-overview-comparison-limitations-and-user-interfaces.html>.
- (85) Imbrioscia, G. M.; Fasoli, H. J. Simulation and study of proposed modifications over straight-parallel flow field design. *Int. J. Hydrogen Energy* **2014**, *39* (16), 8861–8867.
- (86) Kone, J.-P.; Zhang, X.; Yan, Y.; Hu, G.; Ahmadi, G. CFD modeling and simulation of PEM fuel cell using OpenFOAM. *Energy Procedia* **2018**, *145*, 64–69.
- (87) Valiño, L.; Mustata, R.; Gil, M. I.; Martín, J. Effect of the relative position of oxygen–hydrogen plate channels and inlets on a PEMFC. *Int. J. Hydrogen Energy* **2010**, *35* (20), 11425–11436.
- (88) Haghayegh, M.; Eikani, M. H.; Rowshanazamir, S. Modeling and simulation of a proton exchange membrane fuel cell using computational fluid dynamics. *Int. J. Hydrogen Energy* **2017**, *42* (34), 21944–21954.
- (89) Sezgin, B.; Caglayan, D. G.; Devrim, Y.; Steenberg, T.; Eroglu, I. Modeling and sensitivity analysis of high temperature PEM fuel cells by using Comsol Multiphysics. *Int. J. Hydrogen Energy* **2016**, *41* (23), 10001–10009.

- (90) Jourdani, M.; Mounir, H.; El Marjani, A. Modeling a PEM fuel cell under different thicknesses of membrane. *Adv. Appl. Fluid Mech.* **2017**, *20* (4), 605–625.
- (91) Meng, H.; Wang, C.-Y. Large-scale simulation of polymer electrolyte fuel cells by parallel computing. *Chem. Eng. Sci.* **2004**, *59* (16), 3331–3343.
- (92) Weng, F.-B.; Su, A.; Jung, G.-B.; Chiu, Y.-C.; Chan, S.-H. Numerical prediction of concentration and current distributions in PEMFC. *J. Power Sources* **2005**, *145* (2), 546–554.
- (93) Sierra, J. M.; Figueroa-Ramírez, S. J.; Díaz, S. E.; Vargas, J.; Sebastian, P. J. Numerical evaluation of a PEM fuel cell with conventional flow fields adapted to tubular plates. *Int. J. Hydrogen Energy* **2014**, *39* (29), 16694–16705.
- (94) Kahveci, E. E.; Taymaz, I. Assessment of single-serpentine PEM fuel cell model developed by computational fluid dynamics. *Fuel* **2018**, *217*, 51–58.
- (95) Wu, H.-W. A review of recent development: Transport and performance modeling of PEM fuel cells. *Appl. Energy* **2016**, *165*, 81–106.
- (96) Ansys, Inc. *ANSYS FLUENT Fuel Cell Module Manual*; Ansys, Inc.: Canonsburg, PA, 2017.
- (97) Maslan, N. H.; Gau, M. M.; Masdar, M. S.; Rosli, M. I. Simulation of porosity and PTFE content in gas diffusion layer on proton exchange membrane fuel cell performance. *J. Eng. Sci. Technol.* **2016**, *11* (1), 85–95.
- (98) Ibrahimoglu, B.; Yilmazoglu, M. Z.; Celenk, S. Investigation of Spiral Flow-Field Design on the Performance of a PEM Fuel Cell. *Fuel Cells* **2017**, *17* (6), 786–793.
- (99) Zaman, I.; Manshoor, B.; Khalid, A.; Mohamad Sterand, L. A.; Wei Chan, S. Effects of Straight and Serpentine Flow Field Designs on Temperature Distribution in Proton Exchange Membrane (PEM) Fuel Cell. *MATEC Web Conf.* **2016**, *78*, 01116.
- (100) Bilgili, M.; Sivrioglu, M. 3D numerical analysis of PEM fuel cell at different mea thicknesses and operating pressure conditions. *J. Fac. Eng. Archit. Gazi Univ.* **2016**, *31* (1), 51–63.
- (101) Schwarz, D. H.; Djilali, N. 3D Modeling of Catalyst Layers in PEM Fuel Cells. *J. Electrochem. Soc.* **2007**, *154* (11), B1167.
- (102) Wu, X. The influence of active area and stacking on PEM fuel cell performance: A simulation modelling and experimental investigation. Ph.D. Thesis, School of Engineering, RMIT University, Melbourne, Victoria, Australia, 2017; pp 205.
- (103) Patro, D.; Bhattacharyya, S.; Jayaram, V. *J. Am. Ceram. Soc.* **2007**, *90* (10), 3040–3046.
- (104) Li, X.; Fan, X.; Brandani, S. Difference in pore contact angle and the contact angle measured on a flat surface and in an open space. *Chem. Eng. Sci.* **2014**, *117*, 137–145.
- (105) Arif, M.; Cheung, S. C. P.; Andrews, J. A systematic approach for matching simulated and experimental polarization curves for a PEM fuel cell. *Int. J. Hydrogen Energy* **2020**, *45* (3), 2206–2223.
- (106) Min, C. H.; He, Y. L.; Liu, X. L.; Yin, B. H.; Jiang, W.; Tao, W. Q. Parameter sensitivity examination and discussion of PEM fuel cell simulation model validation: Part II: Results of sensitivity analysis and validation of the model. *J. Power Sources* **2006**, *160* (1), 374–385.
- (107) Hu, M.; Gu, A.; Wang, M.; Zhu, X.; Yu, L. Three dimensional, two phase flow mathematical model for PEM fuel cell: Part I. Model development. *Energy Convers. Manage.* **2004**, *45* (11–12), 1861–1882.
- (108) Ashraf Khorasani, M. R.; Asghari, S.; Mokmeli, A.; Shahsmandi, M. H.; Faghish Imani, B. A diagnosis method for identification of the defected cell(s) in the PEM fuel cells. *Int. J. Hydrogen Energy* **2010**, *35* (17), 9269–9275.
- (109) Escobet, T.; Feroldi, D.; de Lira, S.; Puig, V.; Quevedo, J.; Riera, J.; Serra, M. Model-based fault diagnosis in PEM fuel cell systems. *J. Power Sources* **2009**, *192* (1), 216–223.
- (110) Kim, J.; Lee, I.; Tak, Y.; Cho, B. H. State-of-health diagnosis based on hamming neural network using output voltage pattern recognition for a PEM fuel cell. *Int. J. Hydrogen Energy* **2012**, *37* (5), 4280–4289.
- (111) Maizia, R.; Dib, A.; Thomas, A.; Martemianov, S. Proton exchange membrane fuel cell diagnosis by spectral characterization of the electrochemical noise. *J. Power Sources* **2017**, *342*, 553–561.
- (112) Doddathimmaiah, A.; Andrews, J. Theory, modelling and performance measurement of unitised regenerative fuel cells. *Int. J. Hydrogen Energy* **2009**, *34* (19), 8157–8170.
- (113) Guarneri, M.; Alotto, P.; Moro, F. Modeling the performance of hydrogen–oxygen unitized regenerative proton exchange membrane fuel cells for energy storage. *J. Power Sources* **2015**, *297*, 23–32.
- (114) Jin, D.; Ocione, R.; Jiao, K.; Xuan, J. Energy and AI. *Energy AI* **2020**, *1*, 100002.

## ■ NOTE ADDED AFTER ASAP PUBLICATION

This paper was posted ASAP on September 27, 2020, with an incorrect equation citation in the Mass Transport Losses as a Result of the Resistance by the Catalyst Microstructure section. The corrected version was reposted on October 15, 2020.